Geomorphology 478 (2025) 109692

Contents lists available at ScienceDirect

Geomorphology

journal homepage: www.journals.elsevier.com/geomorphology

Reoccupation of late Quaternary relative sea level indicators in a tectonically quasi-stable coastal area in Southern Italy (Cilento headland): Insights into the Last Interglacial stillstands

Vincenzo De Santis [a], Ciro Cerrone [b,*], Marco Meschis [c], Giovanni Scicchitano [a], Alessandra Ascione [d], Massimo Caldara [a]

[a] Department of Earth and Geoenvironmental Sciences, University of Bari, 70125 Bari, Italy
[b] Department of Environmental Sciences, Informatics and Statistics (DAIS), University of Venice Ca' Foscari, Venice, Italy
[c] National Institute of Geophysics and Volcanology, Palermo Section, Palermo, Italy
[d] Department of Earth, Environmental and Resources Sciences (DiSTAR), University of Naples Federico II, Naples, Italy

ARTICLE INFO

Keywords:
Last Interglacial (MIS5e)
MIS 9 and MIS 11
Sea-level reoccupation
Coastal geomorphology
Cilento headland (southern Apennines)

ABSTRACT

A geomorphological-stratigraphical study, integrated with a modelling approach, has been employed to constrain the age of relative sea-level indicators (RSLi) along the quasi-stable Mt. Bulgheria coast in the southern Apennines, located on the eastern margin of the Tyrrhenian Sea. Focusing on the geological evidence of late Quaternary sea-level fluctuations within the 0 to 12 m above sea level (a.s.l.) elevation range, we describe RSLi along ca. 8 km of coastline and constrain their elevation, including those of previously undated RSLi in the same area. The reassessment of field data was needed to address the phenomenon of the reoccupation of older RSLi by younger ones. The approach employs the synchronous correlation method, integrating highstand peak elevations from global sea-level curves and a calibrated uplift rate value, derived from the correlation of RSLi-2 (currently at 8 ± 1 m a.s.l.) with Marine Isotope Stage (MIS) 9c, as suggested by recent findings.

Overall, four RSLi are identified in the investigated coastal zone: RSLi-1 (11 ± 1 m a.s.l.), correlated with MIS 11; RSLi-2 (8 ± 1 m a.s.l.), correlated with MIS 9c and reoccupied during the first MIS 5e peak; RSLi-3 (4 ± 0.5 m a.s.l.) formed during an earlier, undefined stage and reoccupied during MIS 5e; RSLi-4 (2.5 ± 0.5 m a.s.l.) also assigned to MIS 5e. Notably, two cases of reoccupation of older RSLi by younger ones are here reported.

By testing multiple global sea-level curves, we derived a range of possible uplift rates for the chronologically constrained RSLi-2. Consequently, assuming a constant uplift rate throughout the final part of the Middle Pleistocene, we sought the optimal match between all observed RSLi and predicted elevation of palaeo sea levels during past highstands.

The preferred best fit was obtained using a composite eustatic curve from Waelbroeck et al. (2002) and Kopp et al. (2013, for within the MIS5e), and a constant uplift rate of 0.009 mm/yr. Our modelling of MIS 5e (Last Interglacial) identifies three sea-level stillstands and a rapid drop in sea level following the first and highest stillstand. Our results emphasize the importance of the reoccupation problem in sea-level reconstruction studies, especially for RSLi located in regions that are tectonically stable or with relatively low rates of crustal vertical movements. In such contexts, the sea level during younger interglacials may reach or exceed the elevations of older interglacials, reusing or modifying existing RSLi and complicating the identification of which sea-level stand created a specific shoreline feature. The calibrated model supports scenarios where MIS 5e, MIS 9c and MIS 11 had higher peaks than the Holocene (so far). Finally, this work challenges the assumption that RSL indicators ranging between 5 and 8 m a.s.l. in stable regions were exclusively formed during MIS 5e, emphasising the need for precise age constraints in these interpretations.

* Corresponding author.
E-mail address: ciro.cerrone@unive.it (C. Cerrone).

https://doi.org/10.1016/j.geomorph.2025.109692
Received 28 December 2024; Received in revised form 23 February 2025; Accepted 24 February 2025
Available online 3 March 2025

1. Introduction

The interest in Quaternary sea-level oscillations has broadly increased in the last few decades due to the crucial insights they offer into climate dynamics during past interglacials (Montagna et al., 2008), as recently confirmed by the Intergovernmental Panel on Climate Change (IPCC, 2023). Insights on sea-level behaviour during past warm periods are fundamental for unravelling the interaction between natural climatic and anthropogenic influences.

The Last Interglacial (hereafter LIG) corresponds to the Marine Isotope Stage (MIS) 5e, framed between 132 and 116 ka (Kopp et al., 2009; Murray-Wallace and Woodroffe, 2014) within which global mean sea level for several millennia reached a highstand of 5 to 9 m above the modern mean sea level (hereafter a.s.l.) (Kopp et al., 2009; Dutton and Lambeck, 2012; Dutton et al., 2015; Rovere et al., 2016). Relative Sea Level indicators (hereafter RSLi) of the LIG from tectonically stable areas of the Mediterranean have been reconstructed between 2 and 8 m a.s.l. (Benjamin et al., 2017; Cerrone et al., 2021a and reference therein), varying between 2 and 3 m a.s.l. in the Balearic Island of Mallorca (Vesica et al., 2000; Bardají et al., 2009; Lorscheid et al., 2017; Dumitru et al., 2021; Perazzotti et al., 2024) and 7 m a.s.l. along the coasts of the eastern Mediterranean (Sivan et al., 2016). A reliable estimate of the paleo sea level for the entire Mediterranean Sea is 6 ± 3 m a.s.l., with RSLi on the Tyrrhenian coast of Italy at 6.5 ± 1.5 m a.s.l. (e.g., Antonioli et al., 2006; Ferranti and Antonioli, 2007).

In the tectonically stable sectors of the Tyrrhenian coast of Cilento headland, which includes our study area in southern Italy (Fig. 1), Isola et al. (2024) estimated the LIG maximum sea-level highstand at 5.3 m a.

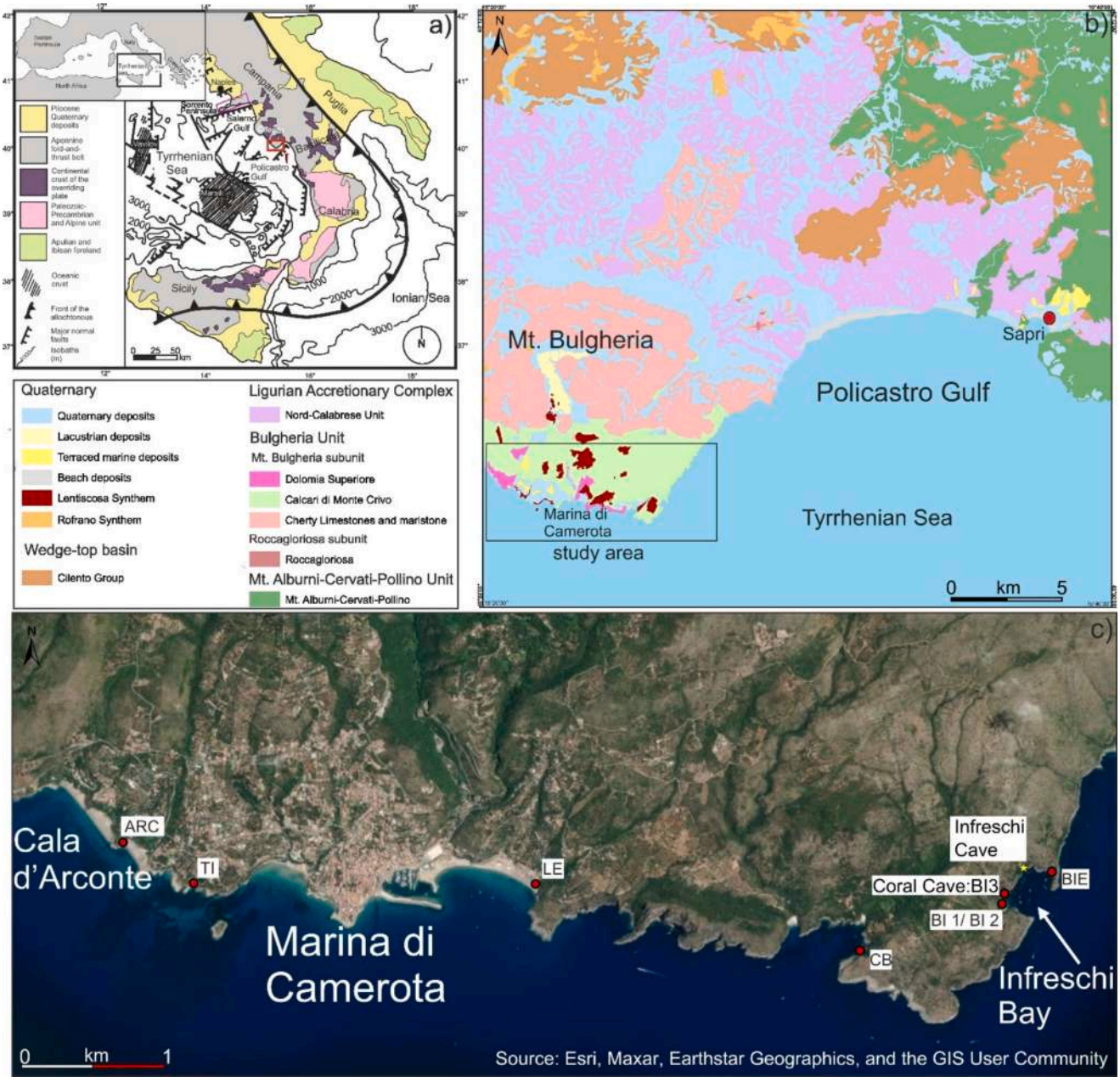

Fig. 1. (a) Tectonic sketch of southern Italy (after Moussat et al., 1986 and Cerrone et al., 2021b); (b) Simplified geological map (after ISPRA, 2016); (c) close-up view of the study area with key outcrops described in this work marked with red circles: ARC = Cala d'Arconte site; TI = Torre dell'Isola site; LE = Lentiscelle site; CB = Cala Bianca site; BI=Baia degli Infreschi sites; BIE = Baia degli Infreschi east site. BI3 site corresponds to Coral Cave, while the Infreschi Cave site, investigated in the works of Esposito et al. (2003), Isola et al. (2024) and Bini et al. (2020) is indicated by a yellow stair.

s.l., consistent with the Dyer et al. (2021) estimation in the Bahamas. However, the duration of the LIG highstand and potential sea level oscillations within the LIG are still debated, with studies suggesting either a single peak (i.e., Dutton et al., 2015), double (i.e., Kopp et al., 2009; Chauveau et al., 2024) and even three or multiple peaks (i.e., Kopp et al., 2013; Rohling et al., 2019) in the 132–116 ka period. Multiple peaks are generally evidenced by sea-level curves derived from field data (i.e., Kopp et al., 2013; Rohling et al., 2019), while they are not reported in the curves derived by $\delta^{18}O$ (e.g., Waelbroeck et al., 2002). Intra-LIG oscillations have also been reported in tectonically stable sectors adjacent to our study area (see Section 2), specifically at the Cilento headland (Fig. 1).

Sequences of RSLi such as staircases of marine terraces or tidal notches, have been studied using the classical sequential method (e.g., Armijo et al., 1996). This method involves assigning an older or younger MIS relative to the elevation of a dated palaeoshoreline. However, many works in the last few decades emphasize the importance of the reoccupation problem in sea-level reconstruction studies, especially for palaeoshorelines located in regions that are tectonically stable or with low rates of crustal vertical movements (e.g., Roberts et al., 2009, 2013; Crosetto et al., 2024). The reoccupation problem occurs whenever sea-level fluctuations reuse or modify existing palaeoshorelines, complicating the determination of which sea-level stand created a particular shoreline feature. This makes it challenging to assign the correct MIS to these indicators based solely on elevation. Indeed, the reoccupation problem arises because the sea level during younger interglacials may reach the same or even higher elevation than those of older interglacials. This is due to the interplay between eustatic changes and glacial isostatic adjustment, and the tectonic behaviour, potentially overprinting geological evidence of the older highstands. Recently, many examples of reoccupation have been described in the Mediterranean (Lambeck et al., 2010; Cerrone et al., 2021b; De Santis et al., 2023; Robertson et al., 2019) and abroad (e.g., Chauveau et al., 2021).

Our study aims to reconstruct sea level oscillations in a coastal sector of southern Cilento (Fig. 1) by integrating: (i) a classical geomorphological and stratigraphical approach based on field mapping of RSLi, and (ii) an age-elevation model of these features. The model works through iteration between global sea level curves (Waelbroeck et al., 2002; Kopp et al., 2013) with an uplift rate calculated based on age constraints from literature data. The age constraints used for the modelling include a recent set of U-series dating on speleothems, which postdate the formation of marine deposits and other erosional RSLi, in the Infreschi Cave, a sea cave next to our investigated area (Isola et al., 2024; Bini et al., 2020).

2. Geological background and previous investigations

The eastern margin of the southern Tyrrhenian Sea basin is characterised by alternating steep rocky cliffs, small sandy pocket beaches, and coastal plains. In particular, the southern side of Mt. Bulgheria (southern Italy), features headlands and narrow bays (Fig. 1). The study area belongs to the fold-and-thrust-belt of the southern Apennines, whose formation is related to the late phases of interaction, which lasted from the Early Miocene to the early part of the Middle Pleistocene (Patacca et al., 1990; Patacca and Scandone, 2001), between the Adriatic and European plates (Malinverno and Ryan, 1986; Patacca et al., 1990; Royden, 1993). Since the late Miocene, thrusting in the chain has occurred simultaneously with the back-arc extension in the Tyrrhenian Sea, driven by the roll-back of the subducting Apulian slab (Faccenna et al., 2001a, 2001b; Malinverno and Ryan, 1986; Royden et al., 1987). Extensional processes migrated eastwards toward the chain, which led to a change in the tectonic regime at Mt. Bulgheria to a stable one. Quaternary extension along the western side of the Southern Apennines is demonstrated by subsidence of coastal grabens such as the Garigliano, Campania and Sele Plains, and coeval uplift of the horst blocks - namely Sorrento peninsula and Cilento headlands - between them (Rehault et al., 1987; Caiazzo et al., 2006 and references therein; Vitale and Ciarcia, 2018 and reference therein; Fig. 1a). At the Licosa Promontory, located in northern Cilento, a wave-cut platform at ca. 5 a.s.l. has been constrained to MIS 5c, while two other wave-cut platforms at ca. 10 m and ca. 6 m a.s.l., along with one at ca. 1.5 m a.s.l., have been correlated with a double peak during the LIG and MIS 5a, respectively (Iannace et al., 2001 and reference therein; Cerrone et al., 2021a). In addition, along the southern side of the Sorrento Peninsula (Fig. 1), Cinque and Romano (1990), Riccio et al. (2001) and Iannace et al. (2003) identified three distinct sets of tidal notches and wave-cut terraces grouped at 7.5–8 m a.s.l., 6.5 m and 3.5 m a.s.l. The entire sequence has been attributed to MIS 5e based on morphostratigraphic correlations, with U-series dating on corals and speleothems providing constraints (Cerrone et al., 2021a and reference therein). In addition, the authors recognised remnants of erosional palaeoshorelines at ca. 2.5 m a.s.l., which they related to either MIS 5a or MIS 5c.

The study area extends from Cala d'Arconte to Baia degli Infreschi (Infreschi Bay) located along the southern side of Mt. Bulgheria, a carbonate massif in southern Cilento (Fig. 1). The massif bounds to the NE margin of the Policastro Gulf and is made up of carbonate rocks ranging in age from the Upper Triassic to the Lower Miocene, forming the Bulgheria tectonic unit (ISPRA, 2016), which is related to the Apennine Platform (Vitale and Ciarcia, 2018). The Bulgheria unit (Upper Cretaceous-Eocene) is further divided into the Roccagloriosa and Mt. Bulgheria tectonic subunits. The Mt. Bulgheria subunit includes the formations of Dolomia Superiore (dolomite) and Calcari di Monte Crivo (limestones) (Fig. 1b, ISPRA, 2016). The Bulgheria unit is tectonically overlain by (i) the Ligurian Accretionary Complex, which consists of the Nord-Calabrese tectonic unit (Cretaceous-lowermost Burdigalian) and the Parasicilide unit (uppermost Cretaceous-Middle Eocene), and (ii) wedge-top basins composed of Lower Miocene-Pliocene siliciclastic sediments (Caiazzo et al., 2006 and reference therein; ISPRA, 2016; Vitale and Ciarcia, 2018). These sediments are considered syn-orogenic deposits, which include the Cilento group (Fig. 1). Finally, the succession is capped by post-orogenic continental and marine deposits, such as the Lentiscosa Synthem (Late Pliocene/Early Pleistocene, ISPRA, 2016), a shallow-water marine unit (Fig. 1), and Quaternary deposits.

In the Cilento area, Mt. Bulgheria is characterised by a staircase sequence of both wave-cut and wave-built marine terraces, ranging from a few metres up to ca. 400 m a.s.l. (Ascione and Romano, 1999). The highest marine surface, located ca. 400 m a.s.l., is attributed to the Santernian substage (Early Pleistocene, 1.8 Ma–1.5 Ma, Cohen and Gibbard, 2019) of the Calabrian stage. Additionally, based on the presence and shape of *Hyalinea balthica*, the terrace at 280 m a.s.l. has been constrained to the Emilian substage (Early Pleistocene, 1.5 Ma-c. 1.2 Ma, potentially MIS 37; Ruggieri and Selli, 1949; Cita et al., 2006; Gibbard and Head, 2009, Cohen and Gibbard, 2019) of the Calabrian stage.

The marine terrace at ca. 150 m a.s.l. is attributed to a generic Middle Pleistocene, based on morpho-stratigraphic records (Ascione and Romano, 1999).

The elevation of RSLi from the Last Interglacial ranges between 5 and 8 m a.s.l. (e.g., Ascione and Romano, 1999; Ferranti et al., 2006; Cerrone et al., 2021a), and indicates that the Cilento area, as well as the nearby Sorrento Peninsula, has been tectonically quasi-stable since at least the Last Interglacial. Since there are no long-term accurate chronological constraints, precise uplift rates estimates for the Middle Pleistocene cannot be made.

Esposito et al. (2003) provided a precise and well-comprehensive description of RSLi from a few tens of km north of Cala d'Arconte to Infreschi Cave. The Authors grouped the recognised five RSLi based on morphostratigraphical correlations and their elevation. In particular, the highest RSLi ranges between 10 and 12 m a.s.l., which they attributed to a generic pre-Tyrrhenian, and other RSLi between 8.5 and 3 m a.s.l., assigned to the MIS 5e-5a interval (Table 1). However, recent research at Infreschi Cave by Bini et al. (2020), which was further

Table 1
The RSLi reported for the study area by Esposito et al. (2003), Isola et al. (2024), and this study.

Esposito et al., 2003	Isola et al., 2024	This study
Evidence between 12 and 10 m a.s.l.	between ca. 9.3 and 8.4 m a.s.l.	RSLi-1: 11 ± 1 m a.s.l. (in site LE and ARC, Fig. 2)
Evidence between 8.5 and 8 m a.s.l.	between ca. 5.9 and 4.4 m a.s.l.	RSLi-2: 8 ± 1 m a.s.l. (in sites LE, TI, CB, BI3, Figs. 2–5)
Evidence between 7.5 and 5 m a.s.l.	between ca. 4.5 and 3.5 m a.s.l.	RSLi-3: 4 ± 0.5 m a.s.l. (in sites LE, TI, CB, BI1, BI2, BI3, Figs. 2–6)
Evidence between 4.5 and 4 m a.s.l.	between ca. 2.5 and 1.7 m a.s.l.	RSLi-4: 2.5 ± 0.5 m a.s.l. (in sites BI3 and BIE, Figs. 2, 5, and 7)
Evidence between 3.5 and 3 m a.s.l.		

updated by Isola et al. (2024), suggests a different scenario. Isola et al. (2024) carried out a morphostratigraphical reconstruction in the coastal sector of Mt. Bulgheria, supported by numerous U-series dating on speleothems, and integrating the age constraints from Bini et al. (2020) for the same area. Isola et al. (2024) assign the upper limit of *Lithophaga* burrows located at 8.35 ± 0.18 m a.s.l. to a paleo sea level predating MIS 7, likely MIS 9c (referred to as MIS 9e by the Authors). Such result is based on evidence that in the Infreschi Cave site the *Lithophaga* burrows are covered by speleothems chronologically constrained by U/Th dating to MIS 6–8 interval. Meanwhile, the highest elevation of the Last Interglacial RSLi was determined to be at 5.3 ± 0.18 m a.s.l. Nevertheless, tidal notches and other morphological indicators below the elevation of the upper limit of *Lithophaga* burrows suggest minor sea level oscillation during the LIG along ca. 12 km of the coast (Isola et al., 2024).

3. Methods

3.1. Field survey

In 2023, field surveys were carried out along the approximately 8 km-long coastline surrounding the southern sector of Mt. Bulgheria, from Cala d'Arconte to Infreschi Bay (Fig. 1c). Infreschi Bay (Fig. 1c) is also the main site of the studies of Bini et al. (2020) and Isola et al. (2024), and is the only site in common to the present work. Nevertheless, with regards to the Infreschi Bay, our study focuses mainly on Coral Cave, while the studies of Bini et al. (2020) and Isola et al. (2024) concentrated primarily on the Infreschi Cave, located at ca. 200 m east of Coral Cave (Fig. 1c). In Esposito et al. (2003), instead, the study focuses on the whole coastal sector of Mt. Bulgheria, and sites in common with our study are: Cala d'Arconte (ARC in Fig. 1), Torre dell'Isola (TI in Fig. 1), Lentiscelle (LE in Fig. 1), Cala Bianca (CB in Fig. 1), and Coral Cave, which is identified as Infreschi Cave in Esposito et al. (2003).

RSLi considered in this work include notches, wave-cut platforms and the upper limit of *Lithophaga* burrows. Their elevation was measured by a Leica DISTO D810 laser measuring device, with an accuracy of 1 mm, and a metered rod with a 10-cm error. These techniques are particularly useful along the Cilento coast due to its topography, with much of the study area characterised by sea caves several tens of metres in height and steep cliffs. RSLi elevations were directly measured relative to the local biological mean sea level (Rovere et al., 2015). In microtidal Mediterranean settings, the biological mean sea level corresponds closely to the mean sea level, with an accuracy of ±0.1 m (Vacchi et al., 2020). The local biological mean sea level has been used in Bini et al. (2020) and, partially, in Isola et al. (2024). In contrast, Esposito et al.'s (2003) elevation is referenced to a generic mean sea level (Table 1).

Through a morpho-stratigraphic correlation conducted in the field, we systematically grouped all site observations and data into four distinct RSLi, providing a clearer framework for analysis.

The elevations of the identified RSLi, along with the associated margin of uncertainty, result from fieldwork aimed at organising a large amount of previous, often contradictory, data (Table 1). These elevation values and their uncertainties vary slightly across the study area. So, the central values reported in this work for each RSLi were derived as the average of the values recorded at the study sites, rounded to the nearest half meter or meter. The uncertainty range was attributed to encompass the maximum and minimum measured values.

The margins of error in our measurement may be attributed to both (i) measurement errors and/or differences in the reference level used to calculate the elevations of RSLi and, (ii) the presence of local RSLi that do not duplicate across multiple sites.

We are aware that the values reported in this study with the associated uncertainty are simplified. This is because we start from the assumption that data with broader areal extent represent the primary RSLi and that these, in turn, are included in the sea-level curves used for our modelling based on the synchronous correlation approach (e.g., Roberts et al., 2009, 2013; Meschis et al., 2024; Varzi et al., 2024).

3.2. The synchronous correlation approach

The sequence of RSLi has been modelled by applying the synchronous correlation method (e.g., Houghton et al., 2003; Roberts et al., 2013, 2009). This method has been largely used within the Mediterranean realm and elsewhere over the past decade, when raised palaeoshorelines and RSLi in general are used to derive uplift rates both in tectonically stable areas (e.g., Pedoja et al., 2018; De Santis et al., 2023, 2021) and tectonically active areas (e.g., Roberts et al., 2013, 2009; Meschis et al., 2022a, 2022b, 2020, 2018; Robertson et al., 2023, 2019; Cerrone et al., 2025). In this work, we consider a "tectonically quasi-stable area" where the mean elevation of an RSL, constrained to the LIG, ranges between 5 and 8 m (Antonioli et al., 2006). The synchronous correlation method is based on the idea that Quaternary sea-level highstands carving raised RSLi in the landscape, are unevenly spaced in time. This implies that RSLi preserved and mapped in the field are unevenly spaced in elevation, for a given uplift rate.

It is important to note that this approach can be adapted to scenarios with either constant or variable uplift rates, as demonstrated by previous investigations (e.g., Roberts et al., 2009; Meschis et al., 2018; Varzi et al., 2024). Furthermore, the synchronous correlation method addresses and highlights the "reoccupation" problem of younger RSLi over older ones, and helps to avoid assigning flawed ages to undated palaeoshorelines when regions with relatively low uplift rates are investigated (e.g., De Santis et al., 2023, 2021; Meschis et al., 2020, 2018; Robertson et al., 2023, 2020, 2019).

The input data of the synchronous correlation method consists of: (i) age and elevation of past sea-level highstands derived from a global sea-level curve, and (ii) a chronological constraint (which may either be from well-established from literature or newly obtained from absolute dating) of at least one RSLi. This combination provides a vertical displacement of the chronologically constrained RSLi and, thus, an uplift rate. So, the synchronous correlation gives a modelled output of current position of past sea-level highstands, that is then compared with the observed RSli elevations, allowing to correlation of local RSLi to global sea-level highstand chronostratigraphy (e.g., Meschis et al., 2020, 2018).

The calculation of the coefficient of determination (R^2) assesses whether a robust correlation exists between mapped RSLi elevations and the calculated current elevations of past sea-level highstands.

For this method, when at least one age control for a raised RSLi is available, the simplest scenario of a constant uplift rate through time is assumed.

If a strong correlation between observations and predictions is not found, scenarios with variable uplift rates over time are tested, following previous studies (e.g. Roberts et al., 2009; Meschis et al., 2022a, 2022b). Alternatively, the observational information may be revisited, and RSLi-diagnostics rechecked.

Different sea-level curves and uplift rate scenarios can also be tested to produce the best match between observed and predicted RSLi.

In the modelling here presented, the first input is a sea-level curve representing the past sea-level highstands, with particular consideration given to their timing and global mean elevation. The second input is the well-established chronological constraint of one RSLi, namely RSli-2 (see Section 4.2), from literature data (Isola et al., 2024).

4. Data and results

In this section, we describe the main RSLi observed in the study area, listed from the highest to the lowest elevations (Table 1, from RSLi-1 to RSLi-4). The bedrock on which the RSLi were carved consists of Triassic limestones and dolomites from the Dolomia Superiore formation and the Calcari di Monte Crivo formation (fm), with some areas featuring marine conglomerates of the Lower Pleistocene related to the Lentiscosa Synthem (Fig. 1).

4.1. RSLi-1 (11 ± 1 m a.s.l.)

Traces of RSLi-1 (Fig. 2), the highest indicator observed in the study area, can be primarily seen at two locations: the cliff bordering Lentiscelle Beach to the east (site LE in Fig. 1c), carved into the Calcari di Monte Crivo fm, and the eastern slope of the promontory where Torre d'Arconte stands (site ARC in Fig. 1c), carved into the Lentiscosa Synthem conglomerates.

At site LE, RSLi-1 is represented by a residual tidal notch at ca. 10.5 m a.s.l., clearly visible on the sides of Serratura Cave (Fig. 2b). At site ARC, RSLi-1 is represented by the inner edge of the wave-cut terrace located at ca. 10–12 m a.s.l.

4.2. RSLi-2 (8 ± 1 m a.s.l.)

This RSLi (Fig. 3) is the best preserved throughout the study area. Therefore, in this section, we describe and present only outcrops with the most significant geomorphological evidence collected during our fieldwork.

On the cliff bordering Lentiscelle Beach to the east (site LE in Fig. 1c), RSLi-2 is represented by the upper limit of a discontinuous band of *Lithophaga* burrows carved into the Calcari di Monte Crivo fm. The band consists of groups of holes, whose upper limit is located at ca. 8 ± 1 m a.s.l. This upper limit coincides with the elevation of the apex of two

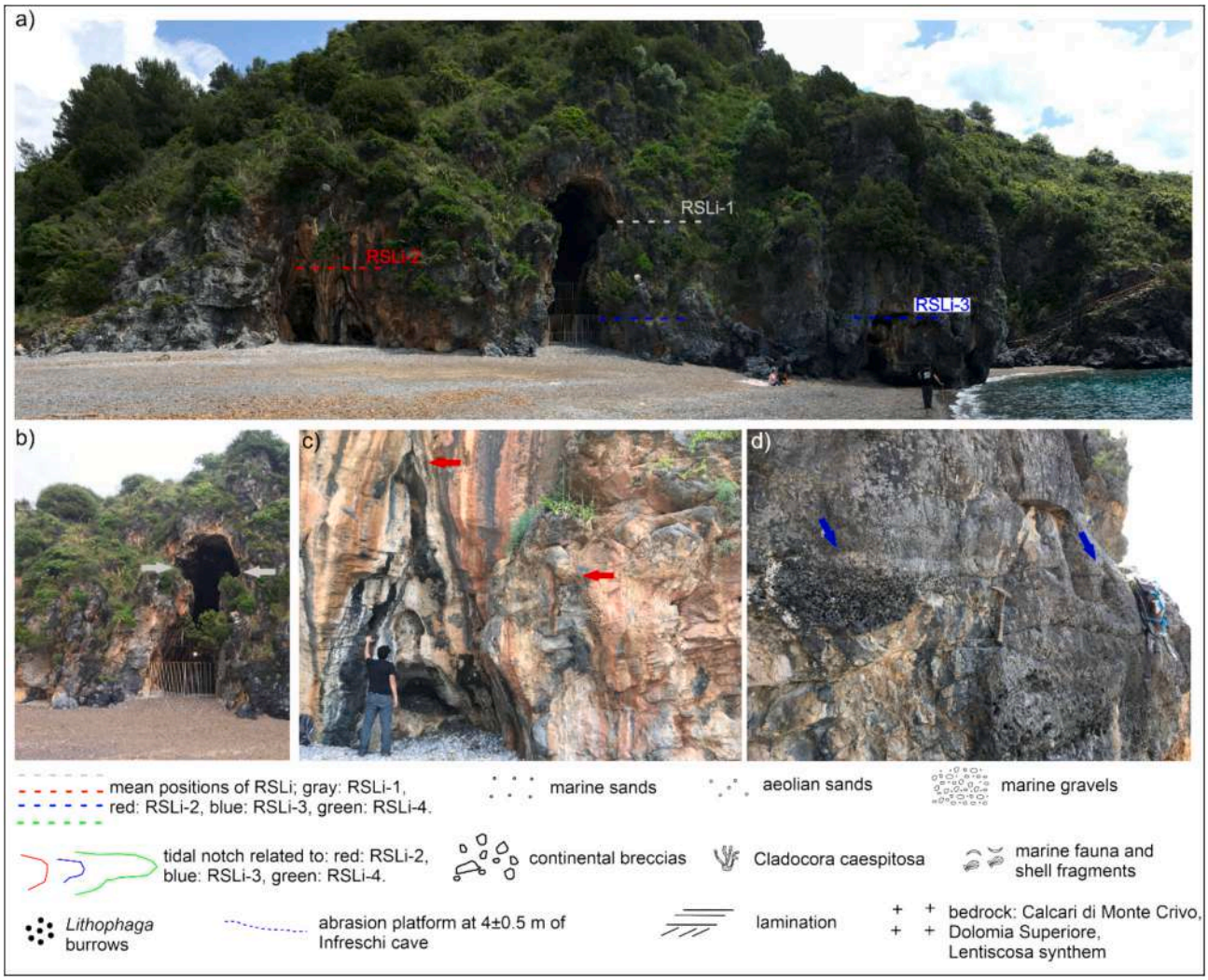

Fig. 2. Site LE (location in Fig. 1c), cliff bordering Lentiscelle Beach to the east. (a) General view showing the recognised RSLi. (b) Close-up view of the residual tidal notch at ca. 10.5 m a.s.l. on both sides of Serratura Cave, representing the local evidence of RSLi-1. (c) Groups of *Lithophaga* burrows (pointed out by red arrows) whose upper limit is at 8 ± 1 m a.s.l., representing the local evidence of RSLi-2. (d) Continuous band of *Lithophaga* burrows, which tend to become smaller toward the upper limit (pointed out by blue arrows), representing the local evidence of RSLi-3. For all the next figures, light grey dotted lines, text, arrows and drawings are associated with RSLi-1, red with RSLi-2, blue with RSLi-3, and green with RSLi-4.

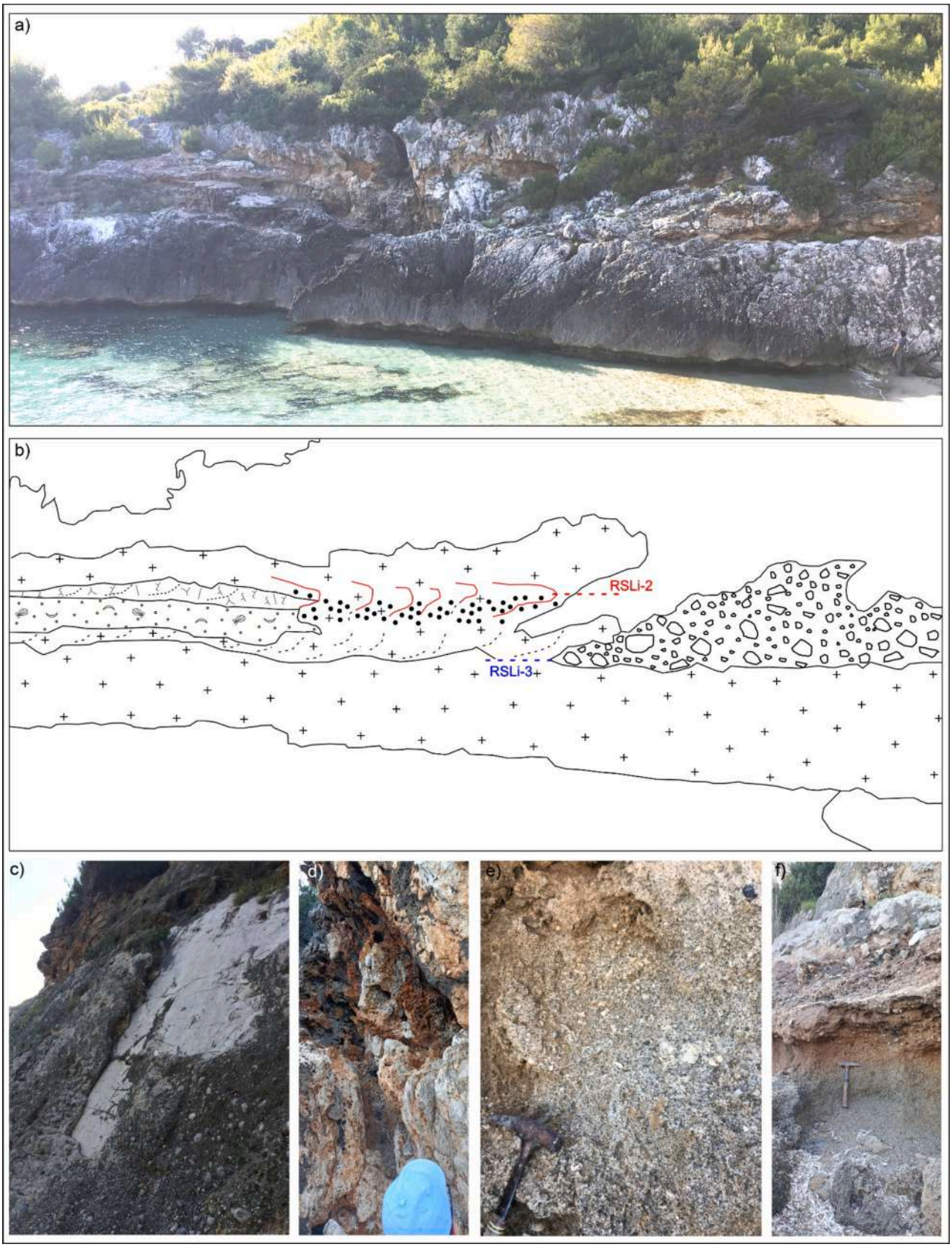

Fig. 3. Site TI, Torre Dell'Isola (location in Fig. 1c). (a) General view of the outcrop. (b) Interpretation. (c) The fault scarp where RSLi-2 and RSLi-3 are modelled. (d) Fairly continuous tidal notch placed at ca. 7.50–7.75 m a.s.l., with *Lithophaga* burrows extending into it, representing the local evidence of RSLi-2. (e) Detail of the marine deposit lying on the narrow, strongly seaward sloping abrasion platform, at about 4 ± 0.5 m a.s.l., made up of coarse, brown-grey, mixed calcarenite-siliciclastic sands with rare marine bivalves. (f) Detail of the passage into reddish continental sand with clear traces of pedogenesis, rich in heterometric, angular, calcareous clasts and crust levels.

grooves on the cliff face (Fig. 2c).

RSLi-2 is also clearly visible on the wall that borders to the west a bay located ca. 250 m west of Torre dell'Isola (site TI; Fig. 3a, b). This wall is likely, at least in part, coincident with a fault scarp (Fig. 3c) that puts in contact the Calcari di Monte Crivo fm (in the footwall) with the conglomerates of the Lentiscosa Synthem (in the hangingwall). At this location, RSLi-2 consists of a continuous tidal notch placed at ca. 7.50–7.75 m a.s.l., with *Lithophaga* burrows extending into it (Fig. 3a, b, d). Below the tidal notch, a narrow abrasion platform can be observed (see RSLi-3 in Section 4.3), partially covered by two different deposits (Section 4.5.2; Fig. 3e, f).

On the sea cliff to the east of Cala Bianca (site CB in Fig. 1c; Fig. 4), RSLi-2 consists of a continuous tidal notch located at ca. 7.90 m a.s.l. with *Lithophaga* burrows within it (Fig. 4a, b). This tidal notch is etched on a sub-vertical wall that can be interpreted as a fault plane formed in the Calcari di Monte Crivo fm. Below the tidal notch, the sub-vertical fault plane is covered by vertically lying clast-supported fault breccia. A platform is incised in this breccia, whose inner margin is at ca. 3.60 m a.s.l. (Fig. 4a; see RSLi-3 in Section 4.3).

In the Infreschi Bay (Fig. 5), on the cliff where Coral Cave opens (site BI3 in Fig. 1c; Fig. 5a), RSLi-2 is a well-defined tidal notch visible on both sides of the upper part of the cave entrance, at ca. 8.50 m a.s.l.; the tidal notch is rich in *Lithophaga* burrows (Fig. 5b). These affect the inner walls of the cave, from ca. 9 m a.s.l. down to a lower platform that forms the cave's floor, located at ca. 4 ± 0.5 m a.s.l. (RSLi-3, see Section 4.3). Upon closer observation, *Lithophaga* burrows within Coral Cave seem to belong to two distinct superposed generations (Fig. 6). The younger (?) *Lithophaga* burrows affect a calcareous crust draping the Calcari di Monte Crivo fm; this crust sometimes contains highly weathered remains of *Cladocora caespitosa* (Linneo) (Fig. 6). The older generation of *Lithophaga* burrows affects also the Calcari di Monte Crivo fm, where it is not covered by the calcareous crust.

Remnants of the tidal notch at 8.50 m a.s.l. are visible along the stretch of cliffs at Infreschi Bay between Coral Cave and Infreschi Cave (Fig. 5c).

4.3. *RSLi-3 (4 ± 0.5 m)*

This RSLi is well-preserved throughout the study area and, in this section, we describe and show the key outcrops.

On the cliff bordering Lentiscelle Beach to the east (site LE in Fig. 1c; Fig. 2), carved into the Calcari di Monte Crivo fm, RSLi-3 is represented

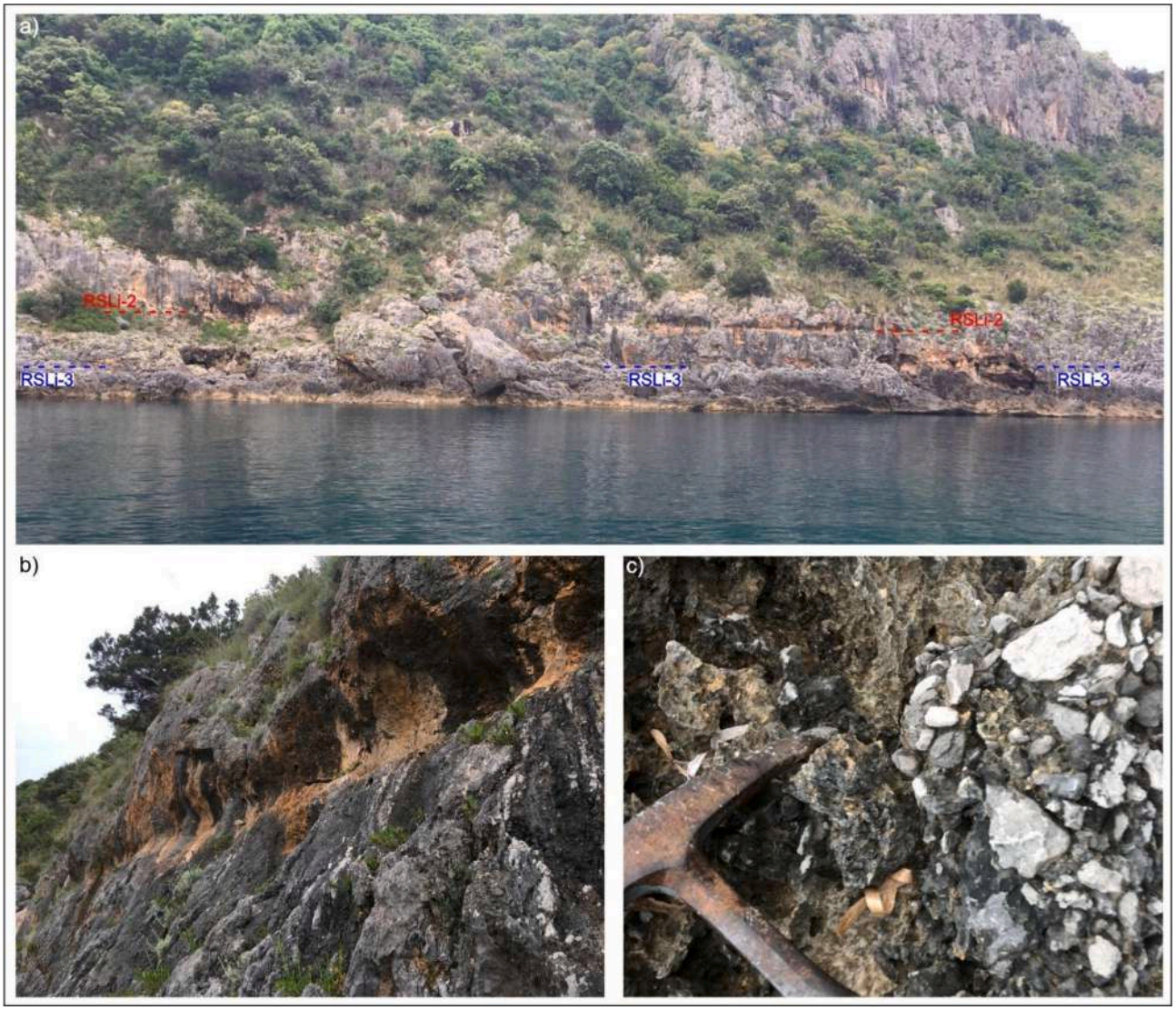

Fig. 4. Site CB, Cala Bianca (location in Fig. 1c). (a) General view with the position of RSLi-2 and RSLi-3, here represented respectively by a continuous tidal notch located at ca. 7.90 m a.s.l. and by a platform a few meters wide, with a highly irregular surface and inner margin at ca. 3.6 m a.s.l. (b) Detail of the tidal notch of RSLi-2. c) detail of the small colony of *Cladocora caespitosa* (Linneo) found on the platform of RSLi-3.

Fig. 5. Infreschi Bay, where sites BI1, BI2, and BI3 are (location in Fig. 1c). Site BI3 corresponds to Coral Cave and its immediate surroundings. (a) Coral Cave and its surroundings with RSLi-2, RSLi-3, and RSLi-4. The dotted black rectangle represents the area reported in more detail in Fig. 8. (b) Close-up view of the tidal notch with *Lithophaga* burrows representing RSLi-2 seen from inside the Coral Cave; toward the foreground, in the left side, a continental deposit of unit U4 mantle the wall of the cave. (c) General view of the sector of Infreschi Bay between Coral Cave and Infreschi Cave, with red arrows pointing out the well-preserved portions of the tidal notch of RSLi-2. (d) Continuous band of *Lithophaga* burrows, located at ca. 3.5–3.7 m a.s.l., representing RSLi-3 at site BI1; the blue arrows point out its upper limit. On the right of the figure, the cave notch of Fig. 5e can be seen. (e) Cave notch with an abrasion platform in front representing RSLi-3 at site BI3, which is contiguous to BI1; the blue arrows indicate the upper limit of *Lithophaga* burrows.

by the upper limit of a continuous band of *Lithophaga* burrows, at ca. 3.5 m a.s.l. The burrows tend to become smaller toward the upper limit, which appears sharp (Fig. 2d).

At Cala Bianca (site CB in Fig. 1c, Fig. 4), below the continuous tidal notch RSLi-2 at 7.90 m a.s.l. (Section 4.2), RSLi-3 is represented by a platform at most a few meters wide, with a highly irregular surface, incised in a vertically lying clast-supported fault breccia. The inner margin of this platform is at ca. 3.6 m a.s.l. A marine deposit a few cm

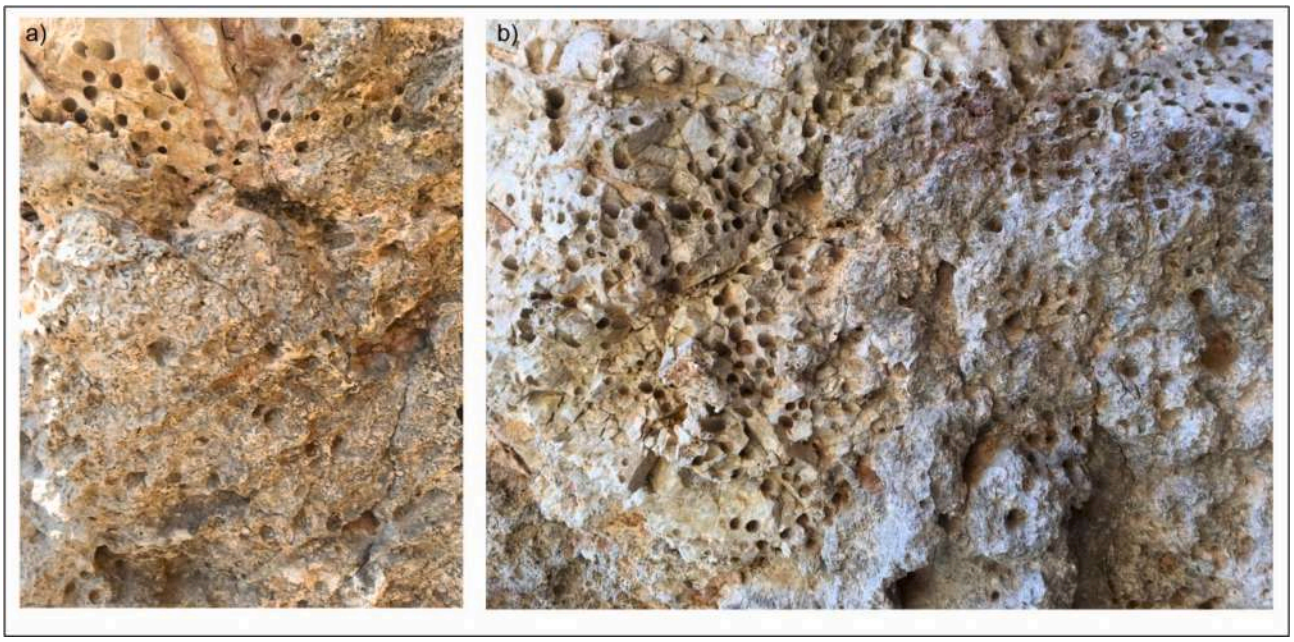

Fig. 6. Coral Cave (site BI3; location in Fig. 1C). Note: (a) the generation involving the calcareous crust containing weathered remains of *C. caespitosa*, and (b) the two generations of *Lithophaga* burrows visible in the inner walls of the cave.

thick, consisting of yellowish, coarse sand containing scattered decimetric to centimetric calcareous clasts, generally angular to subrounded, is present on this platform in small, discontinuous patches. This deposit contains rare specimens of *Bolma rugosa* (Linneo); a small in situ colony of *C. caespitosa*, highly recrystallized as indicated by XRD analyses (Prof. Giuseppina Balassone, pers. comm.), was also found (Fig. 4c).

At Torre dell'Isola (site TI; Fig. 3), RSLi-3 appears as a narrow, strongly seaward sloping abrasion platform, modelled on the Calcari di Monte Crivo fm, set at about 4 ± 0.5 m a.s.l., partially occupied by both marine and continental deposits (Fig. 3d, e, f; see Section 4.5.2).

Evidence of RSLi-3 is present throughout the Infreschi Bay (sites BI1, BI2, BI3; Fig. 5). At sites BI1 and BI2 (Fig. 5d, e), RSLi-3 is recognizable in the upper limit of a continuous band of *Lithophaga* burrows, located at ca. 3.5–3.7 m a.s.l. (Fig. 5d). Laterally, RSLi-3 transitions into a cave notch in which *Lithophaga* burrows are visible, with abrasion platform in front (Fig. 5e).

At Coral Cave (site BI3; Fig. 5a), RSLi-3 is represented by an abrasion platform, shaped in the Calcari di Monte Crivo fm. This platform forms the floor of the cave and is located at an elevation ranging from 3.5 to 4.5 m a.s.l., considering both the cave and its immediate surroundings. Near the Coral Cave, the platform passes laterally to tidal notches and/or cave notches with *Lithophaga* burrows (Fig. 5a).

4.4. RSLi-4 (2.5 ± 0.5 m)

RSLi-4 is not well preserved. It generally consists of cave notches at ca. 2.5 m a.s.l. (see Fig. 5a) and small remnants of abrasion platforms with inner margins at ca. 2.5 ± 0.5 m, which are present throughout the study area. The best outcrops are located at Cala Bianca and Infreschi Bay.

At Cala Bianca, a few tens of metres SW of the site CB (palaeo RSLi-2; Section 4.2), there is an abrasion platform with good lateral continuity, slightly seaward-sloping and carved into the Calcari di Monte Crivo fm, whose inner margin is ca. 2.5 m a.s.l.

In the eastern sector of Infreschi Bay (site BIE; Fig. 7), RSLi-4 consists of a quasi-horizontal abrasion platform carved into the Calcari di Monte Crivo fm. The inner margin of this platform transitions, slightly higher up, into a discontinuous tidal notch located at ca. 2.5 m a.s.l. (Fig. 7a, b), partially filled by marine deposits and drilled by *Lithophaga* burrows (Fig. 7c). Patches of marine deposits (described in the following Section 4.5.3) are present onto the platform.

4.5. Deposits associated with the analysed RSLi

In this section, we describe in detail the deposits associated with the RSLi that are most significant to the reconstruction of both the morphostratigraphical setting and the geomorphological evolution of the study area.

4.5.1. Deposits of Coral Cave

At Coral Cave (Section 4.2), the *Lithophaga* burrows are present seamlessly up to ca. 8.5 m a.s.l. On the platform which forms the floor of the cave and ranges in elevation from 3.5 to 4.5 m a.s.l. (RSLi-3; Fig. 5a), there is a succession of deposits (Fig. 8). These deposits are grouped in the following units, listed from bottom to top:

1) U1. It consists of a clast-supported pebbly deposit, with a scarce coarse sand matrix. Clasts are calcareous in nature, poorly sorted, and range from subrounded to subangular. Deposit U1 contains *Patella caerulea* Linneo, *Spondylus gaederopus* Linneo, *Manupecten pesfelis* (Linneo), *Mimachlamys varia* (Linneo), *Patella* sp., *Cladocora caespitosa* (Linneo). This unit, which is indicative of a high-energy beach, can be interpreted as coeval to the formation of the wave-cut platform.
2) U2. Above the pebbly deposit of U1, isolated patches of coarse, well-cemented mixed siliciclastic-calcareous arenite are found. These patches contain isolated subrounded to subangular pebbles and/or fine, well-rounded gravels, along with small, indeterminable bioclasts. This deposit drapes a bioherm of *C. caespitosa*, ca. 30–40 cm high, located roughly in the centre of Coral Cave's entrance. Deposit U2 can be interpreted as a syn wave-cut platform deposit, indicative of a high-energy beach. The arenitic-gravelly deposit postdates the bioherm of *C. caespitosa*. XRD analysis of *C. caespitosa* samples reveals a high concentration of calcite (Prof. Giuseppina Balassone, University of Naples Federico II, pers. comm.), indicating a post-mortem diagenesis where the original aragonitic shells have transformed into calcite.

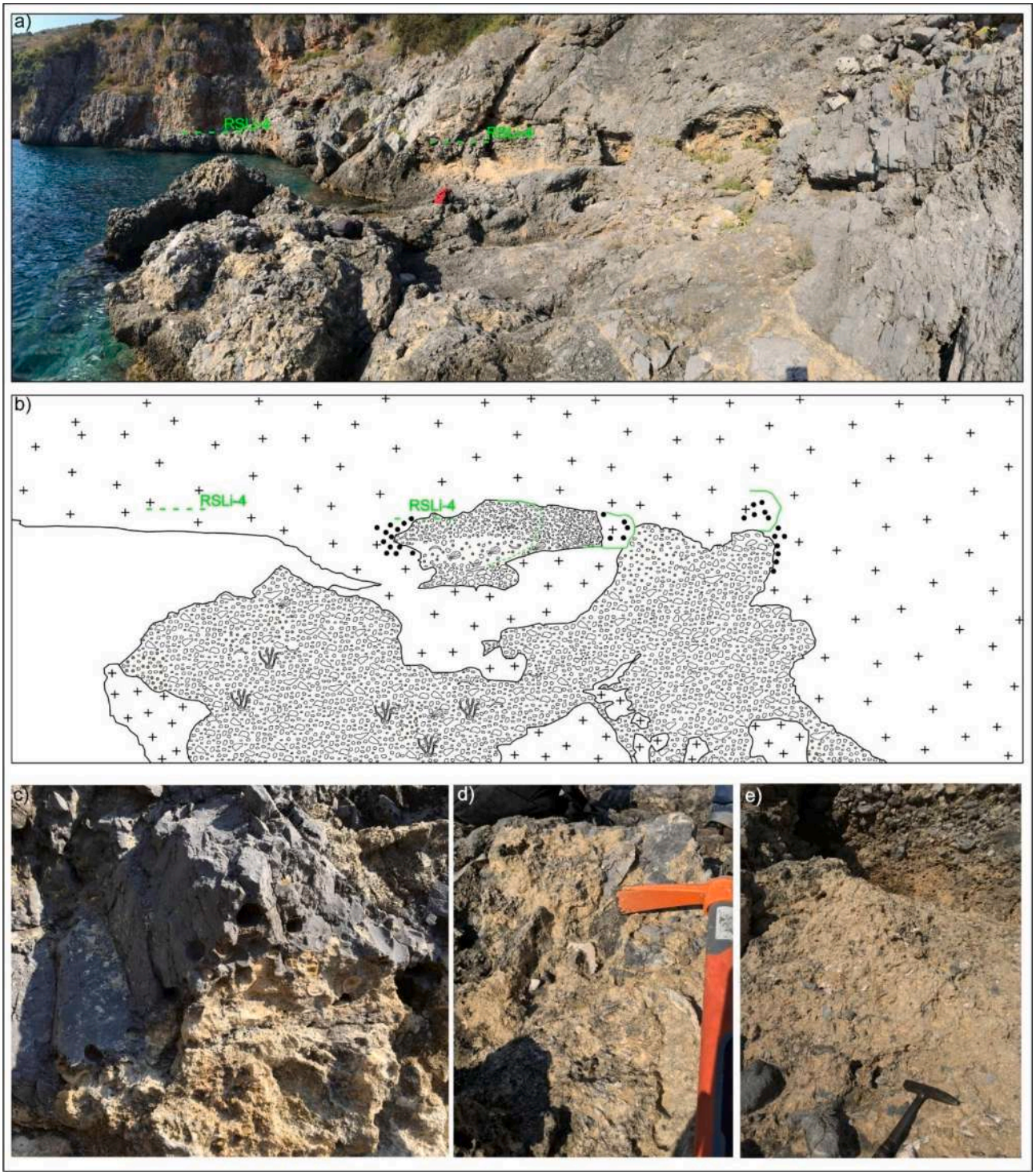

Fig. 7. Baia Infreschi east (site BIE, location in Fig. 1c). (a) Panoramic view of BIE site. (b) schematic sketch of the outcrop in BIE site. (c) *Lithophaga* burrows at the inner margin of the platform. (d) *C. caespitosa* within the deposit lying on the platform. (e) Close-up view of the yellowish calcarenite with subangular clasts lying on the RSLi-4 platform, containing bivalves.

3) U3. Above U1 and U2, there is a deposit consisting of well-sorted, medium-fine tawny-yellowish laminated sands. The sands are strongly cemented and exhibit a subhorizontal to slightly sloping inclination toward the interior of the cave. They are devoid of macrofauna and partially drape the lower part of the cave walls. This deposit can be interpreted as sands of aeolian origin.
4) U4. Above the fine sands of U3, toward the inner part of the cave, a continental deposit is found. The deposit consists of a reddish-brown sandy soil containing angular to subangular heterometric calcareous clasts. It gradually thickens toward the inner edge of the cave, where it merges with the cave roof. Additionally, a thin, yellowish sandy-silty layer within deposit U4 is interpreted as a pyroclastic deposit by Filocamo (2000). Deposit U4 is regarded as indicative of a continental environment.

All of the depositional units identified in Coral Cave overlie the

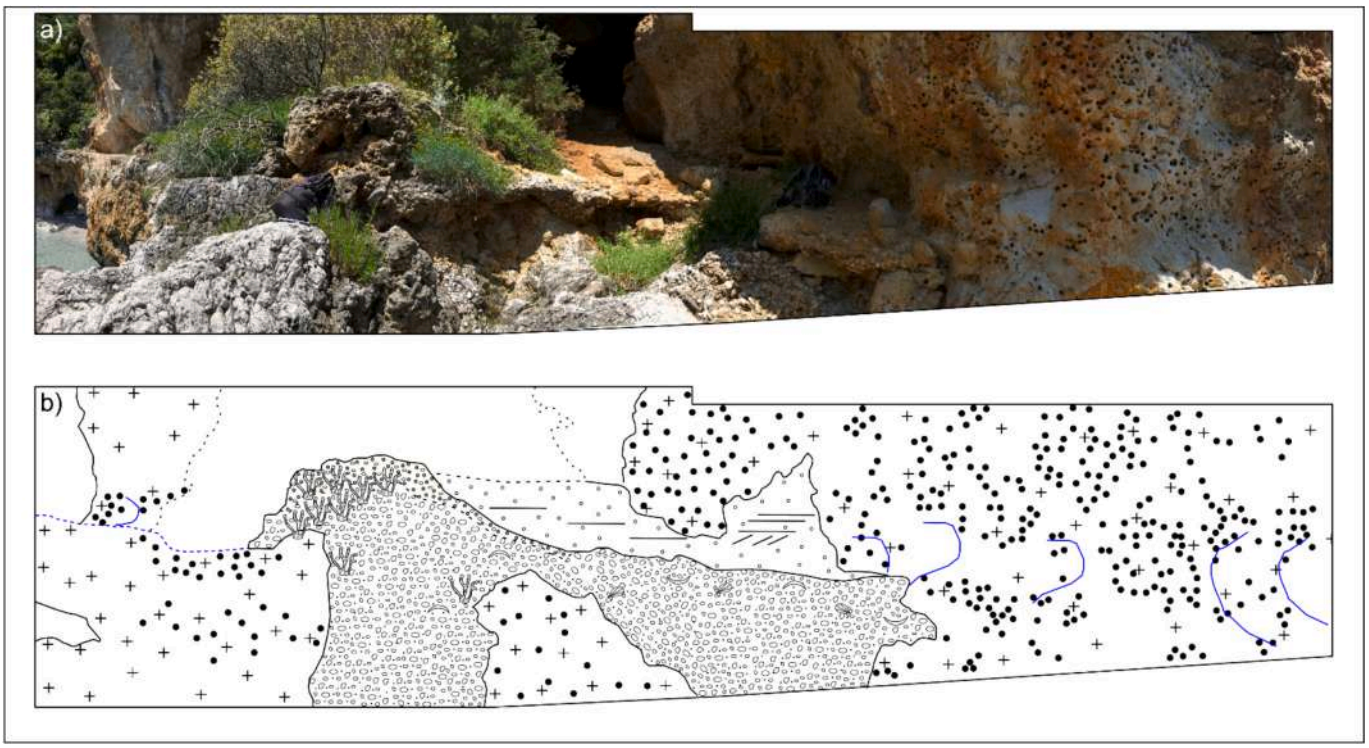

Fig. 8. Deposits at the entrance of Coral Cave (see black dotted rectangle in Fig. 5): (a) outcrop; (b) interpretation. Blue colour highlights all the landforms related to RSLi-3 (tidal notch and abrasion platform, it is not covered by deposits).

Lithophaga burrows found on the cave walls and floor, suggesting that they are younger than the burrows.

4.5.2. Deposits of Torre dell'Isola (TI)

Below the tidal notch at ca. 7.50–7.75 m a.s.l., the strongly seaward sloping abrasion platform at ca. 4 ± 0.5 m a.s.l. related to RSLi-3 (Fig. 3b) is partially covered by two different deposits (Fig. 3b). Toward the outer side of the bay, there is a deposit composed of coarse, brown-grey, mixed calcarenitic-siliciclastic sands with subhorizontal stratification and rare marine bivalves, including *Tetrarca tetragona* (Linneo), *Barbatia barbata* (Linneo), *Mimachlamys varia* (Linneo), *Diodora graeca* (Linneo), *Patella caerulea* Linneo, *Patella* spp. The upper part of these sands is reddish-brown (Fig. 3f). Toward the top, it gradually transitions into a reddish continental sand with clear traces of pedogenesis, rich in heterometric, angular, calcareous clasts (Fig. 3f). Within this layer, worked lithic fragments (flint), femic minerals, and levels of calcareous concretions are present.

Toward the inner side of the bay, the deposit consists of breccias and conglomerates with heterogeneous and heterometric clasts (centimetric to metric in size) embedded in a matrix of reddish sands and silts (Fig. 3b).

4.5.3. Deposit of Baia degli Infreschi est (BIE)

In the eastern sector of Baia degli Infreschi (BIE site; Fig. 7), the RSLi-4 subhorizontal abrasion platform carved into the Calcari Monte Crivo fm terminates at a discontinuous tidal notch at ca. 2.5 m a.s.l. A marine deposit partially fills the innermost part of this platform, consisting of a coarse, clast-supported conglomerate with subrounded, centimetric to decimetric calcareous clasts. This conglomerate is what partially fills the edges of the tidal notch (Fig. 7a, b). Toward the outer margin, the deposit covers the abrasion platform in patches. It is composed of a coarse, clast-supported conglomerate with subrounded to subangular, centimetric to decimetric calcareous clasts, and sections of a cemented yellowish calcarenite, containing subrounded to subangular. The deposit contains *Spondylus gaederopus*, *Chlamys varia*, *Ostrea* sp., *Balanus* sp., and highly recrystallized *C. caespitosa* (Fig. 7d, e), along with numerous indeterminate mollusc fragments.

4.6. Results from the synchronous correlation approach

Field evidence we surveyed in the first ca. 12 m a.s.l. suggests a complex history of the relative sea level oscillations for southern Cilento (Fig. 6), in agreement with previous investigations at Infreschi Cave (Bini et al., 2020; Isola et al., 2024). However, there are no direct age controls for the mapped RSLi, such as the upper limits of *Lithophaga* burrows and fossil tidal notches. So far, the only chronological constraints are based on a series of U/Th dating on speleothems, which have indirectly established a relative chronology for RSLi recognised in the study area (Bini et al., 2020; Isola et al., 2024). Thus, the synchronous correlation method (Section 3.2) provides a viable approach for determining ages to undated RSLi.

Our model is driven by the assumption that RSLi-2 belongs to MIS 9c, according to the conclusions of Isola et al. (2024). Indeed, Isola et al. (2024) recognise, in the Infreschi Bay, an upper limit of *Lithophaga* burrows at 8.35 m a.s.l. The Authors recognise the same upper limit along the Cilento coast, specifically at Marina di Camerota ("Spiaggia di Peppe" site) and at Palinuro Harbour, where they measured elevations of 8.6 ± 0.1 m and 8.8 ± 0.1 m a.s.l., respectively. We have correlated this upper limit with our RSLi-2, which we have measured at 8 ± 1 m a.s.l. in several localities of the study area (Fig. 1c).

We tested several sea-level curves. A first plausible scenario was obtained using, as input for the synchronous correlation method (Section 3.2), the sea-level curve of Waelbroeck et al. (2002). Thus, adopting the correlation of RSLi-2 with MIS 9c, we have considered that, according to Waelbroeck et al. (2002), MIS 9c was attained at. ca. 330 ka, when the sea level reached an elevation of 5 m a.s.l. Since the mean current elevation of RSLi-2 is at 8 m a.s.l., the mean vertical displacement is 3 m within 330 ka, resulting in a mean uplift rate of 0.009 mm/yr. This uplift rate has been assumed to be constant since the final part of the Middle Pleistocene, based on literature data that estimate a final

Middle Pleistocene uplift, although no numerical rate has been calculated (Ascione and Romano, 1999).

Nevertheless, this simulation could not justify and assign ages to all RSLi we have recognised in the field (Supplementary material 1). Using exclusively the sea-level curve from Waelbroeck et al. (2002), which is derived from $\delta^{18}O$ data, the field-measured RSLi at a mean elevation of 4 m a.s.l. remains unassigned, as it shows a poor fit with this model.

Aimed at assigning ages to all observed RSLi up to 12 m a.s.l., we integrated the sea level curve of Waelbroeck et al. (2002), replacing, only for the LIG (132–116 ka), the values with the sea-level stillstands from Kopp et al. (2013). This resulted in a composite sea-level curve of the final preferred best-fitting scenario (which maintains the uplift rate of 0.009 mm/yr, assumed as constant) reconstructed as shown in Table 2. This choice was driven by: (i) field evidence from our study sites which suggest multiple sea-level oscillations during the LIG (Section 4: RSLi-2, RSLi-3 and RSLi-4), in broad agreement with some consideration made by Isola et al. (2024) as indirect result of their chronological constraints; and (ii) the inability of traditional global sea level curves based on $\delta^{18}O$ (e.g., Waelbroeck et al., 2002) to resolve these intra-LIG oscillations.

We associated the expected RSLi elevations (generated by the synchronous correlation method) with the observed RSLi elevations (4th column of Table 2) by finding the best match between them. Hence, we obtained a coefficient of determination (R^2) value of 0.98 (Fig. 9).

It is important to note that, given the sea-level maximum uncertainty of ±13 m in Waelbroeck et al. (2002) (sigma not specified), and a sea-level maximum confidence interval of ca. 13 m in Kopp et al. (2013) (2-sigma), we may consider acceptable a gap of up to 10 m between predicted and the observed RSLi elevations (compare the 3rd and 4th columns in Table 2).

We finally highlight that we identified four RSLi between 118 ka and 410 ka with intra-LIG oscillations, similar to previous investigations within the Mediterranean realm regardless of the influence of tectonic processes (Cinque and Romano, 1990; Riccio et al., 2001; Iannace et al., 2003; Roberts et al., 2013; Meschis et al., 2018, 2022a, 2022b; Robertson et al., 2019, 2023; De Santis et al., 2021, 2023). In particular, our modelling results (Table 2, Table 3, and Fig. 10) show that RSLi-1 should be correlated with MIS 11 (410 ka). In addition, the results suggest that RSLi-2, which is correlated with MIS 9c (330 ka), was reoccupied by the older and first intra-LIG highstand (124 ka). Furthermore, RSLi-3 should belong to the younger intra-LIG stillstand (118 ka) which has reoccupied an older, undated palaeoshoreline, as suggested by morpho-stratigraphic and paleoecological features (see Section 5.2), while RSLi-4 should belong to the middle intra-LIG stillstand (120 ka) (Tables 2 and 3, and Fig. 10).

Table 2
Ages and sea-level elevations of highstands, both from Waelbroeck et al. (2002) and Kopp et al. (2013, only for LIG), in 1st and 2nd columns, respectively. 3rd column: Predicted RSLi (m) elevations by applying the synchronous correlation method. It is based on chronological constraint that RSLi-2 at 8 ± 1 m a.s.l. dates to MIS 9c (Isola et al., 2024), attained at ca. 330 ka with a sea-level at 5 m a.s.l. (Waelbroeck et al., 2002), and resulting vertical displacement of 3 m and uplift rate of 0.009 mm/y.

Ages of highstands/ stillstands (yrs)	Sea-level relative to today (m)	Predicted elevations of RSLi (m)	Field-measured RSLi (mean values, in metres)
0	0	0	0
30,000	−80	−80	
50,000	−60	−60	
80,000	−19	−18	
100,000	−20	−19	
118,000 (MIS 5e, "last")	3	4	4 (RSLi-3)
120,000 (MIS 5e, "intra")	−0.5	1	2.5 (RSLi-4)
124,000 (MIS 5e, "first")	7	8	8 (RSLi-2)
166,000	−50	−49	
196,500	−10	−8	
215,000	−4	−2	
235,000	−12	−10	
287,000	−15	−12	
303,000	−15	−12	
330,000 (MIS 9c)	5	8	8 (RSLi-2)
410,000 (MIS 11)	6	10	11 (RSLi-1)

Before choosing the modelling scenario based on the combination of the sea-level curves of Waelbroeck et al. (2002) and Kopp et al. (2013), we tested different other sea-level curves and, consequently, different uplift rate scenarios over time. For instance, we tested the curve by Spratt and Lisiecki (2016), with and without the inset of Kopp et al. (2013) for the LIG (Supplementary material 2). The main problem in the use of this curve is that the reconstructed sea level of MIS 11 is at ca. 16 m a.s.l. In fact, in the Spratt and Lisiecki (2016) sea-level curve, to our reference MIS 9c peak is assigned an elevation at approximately the same level as today, and an age of ca. 328 ka. This would imply an uplift rate of ca. 0.027 mm/y for the study area and, as a consequence, an expected elevation for the MIS 11 RSLi of ca. 27 m a.s.l. However, we found no field evidence of a paleo sea-level stand at this elevation (Supplementary material 2).

The value of the coefficient of determination (R^2), calculated for the composite sea-level curve of Waelbroeck et al. (2002) and Kopp et al. (2013) is the highest obtained from a scenario which allows to assign all observed RSLi to past sea-level stillstands. It suggests that our geomorphological analysis is robust enough to be used for deriving implications regarding the Late Pleistocene sea-level changes from MIS 11 to LIG.

5. Discussion

5.1. RSLi reconstruction and their reoccupations

In the investigated 0 to 12 m a.s.l. elevation range, we identified the geomorphological-stratigraphical record of multiple sea-level fluctuations that affected the coastal belt of Mt. Bulgheria. Dating of the RSLi, which are represented mainly by erosional features such as upper limits of *Lithophaga* burrows and fossil tidal notches, has been hindered by the absence of sedimentary material suited for dating. Indeed, although fossil corals like *C. caespitosa* are fairly common in the study area, diagenetic processes hampered obtaining reliable age constraints. To date, the best chronological constraints come from U/Th dating on speleothems, which have provided a relatively broad, yet the best available, chronological range for the RSLi in the study area (Esposito et al., 2003; Bini et al., 2020; Isola et al., 2024). Using those chronological constraints, we modelled RSLi in the Mt. Bulgheria coastal area.

Our modelling suggests a correlation of the analysed RSLi with MIS 11 to 5. Worthy to note, our results suggest the constancy of uplift rate in the study area and in the investigated time interval. Therefore, it appears that the Mt. Bulgheria area has become quasi-stable from MIS 11.

Field evidence indicates that some RSLi have been reoccupied by younger sea level rises, resulting in either partial or complete overprinting of the older features. Therefore, our study area could serve as an ideal test site for studying and interpreting coastal landforms shaped by multiple sea-level stillstands in a quasi-stable region during the Quaternary (Ferranti et al., 2006).

In particular, the results of our study suggest that the first and older sea-level highstand belonging to the MIS 5e (as defined by Kopp et al., 2013) has reoccupied the position of the 330 ka old MIS 9c sea-level highstand (Table 3). This implies that the present-day RSLi-2 reflects a more complex history involving both sea-level changes and relatively low and modest rates of crustal deformation. Additionally, the third sea-level highstand of MIS 5.5 (as defined by Kopp et al., 2013) has reoccupied an older, undefined RSLi (Table 3), as indicated by ecological, geomorphological, and geological evidence (discussed in the next Section 5.2). Thus, the present-day RSLi-3 also results from a similarly complex history of interaction between sea-level changes and relatively

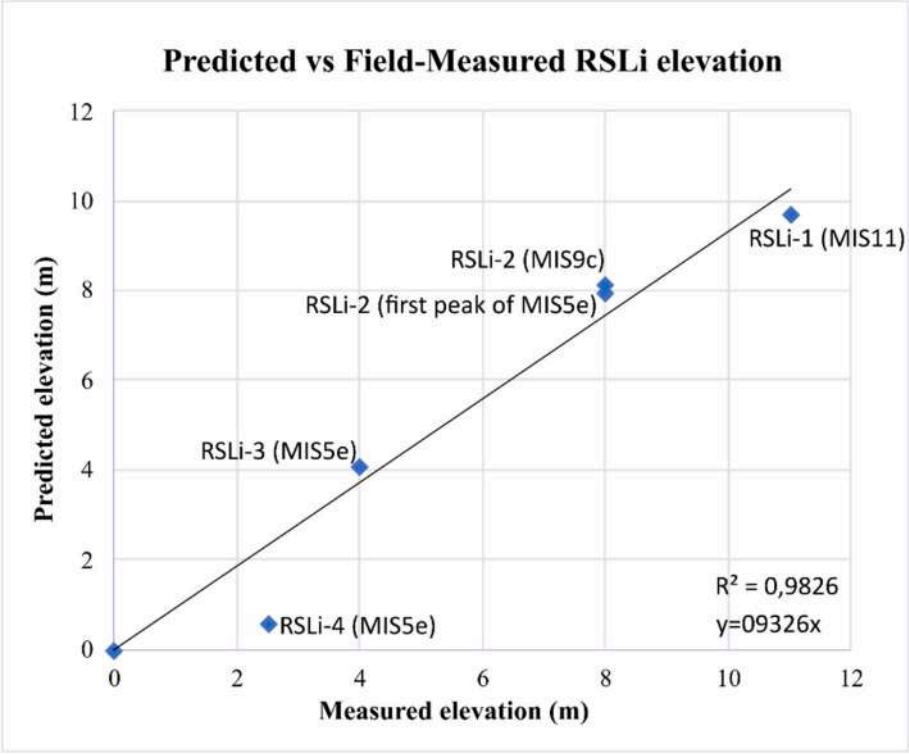

Fig. 9. Graph depicting the comparison between observed and expected RSLi elevations (Table 3). Good fits are indicated by R^2 values ≥0.98.

Table 3
Age model for the RSLi with the proposed age, which comes from the synchronous correlation method and correlation with Marine Isotope Stages.

RSLi		Age proposed (ka)	Marine isotope stage
Label	Elevations (m)		
RSLi-1	11 ± 1	410	MIS 11
RSLi-2	8 ± 1 m	330 and 124	MIS 9c and MIS 5e
RSLi-3	4 ± 0.5 m	118	MIS 5e and another older undefined stage
RSLi-4	2.5 ± 0.5 m	120	MIS 5e

low rates of crustal deformation.

5.2. *The problem of RSLi-3 in the Infreschi Bay and evidence of its reoccupation*

Field evidence suggests that RSLi-3 may result from the reoccupation of an older palaeo sea-level stillstand by a late sea-level stillstand of MIS 5e. This inference is supported by ecological, geomorphological and geological data related to RSLi-3 observed in Infreschi Bay, particularly at Coral Cave (Fig. 1c; Fig. 8). We refer in particular to the presence of a *C. caespitosa* bioherm above the platform at 4 ± 0.5 m a.s.l., which represents RSLi-3, in front of the Coral Cave entrance (Fig. 8). Our model indicates that RSLi-3 is correlated with the last sea-level peak of MIS 5e (c. 118 ka, Table 1). Nevertheless, the *C. caespitosa* bioherm above the platform is incompatible with a sea level at that position, because this would imply that the bioherm formed in an intertidal environment, subject to frequent wave action of the surf zone. However, literature data on living *C. caespitosa* in the Mediterranean indicate that this coral is typically found starting from 4 to 5 m below the sea level (Kružić and Požar-Domac, 2003; Peirano et al., 2003). Thus, when the third MIS 5e sea-level stillstand was forming RSLi-3 (around 118 ka), the *C. caespitosa* bioherm most likely already existed, and consequently, the platform on which it lies predates the 118 ka old event (Fig. 10a).

A possible scenario to explain morpho-stratigraphical evidence from Coral Cave implies that during the MIS 5e transgression, the platform at 4 ± 0.5 m a.s.l. already existed (Fig. 10a). As the sea level rose and reached this pre-existing platform during the transgression toward the peak of MIS 5e, it is likely that unit U1 was deposited (Fig. 10b). Then, the *C. caespitosa* bioherm formed above U1 during the last phase of sea level rise and the first highstand of MIS 5e, which culminated at 124 ka according to our model (Table 1, using timing of Kopp et al., 2013). At 124 ka, the sea level was at the RSLi-2 position, fully submerging the platform with an estimated water depth of ca 4 m (Fig. 10c). Following our correlative modelling, the sea level subsequently dropped to the RSLi-4 position (Fig. 10d), around 120 ka. During this phase, the *C. caespitosa* bioherm may have undergone early diagenesis and erosion in a subaerial environment. Later, around 118 ka, the sea level rose again, reoccupying the platform at 4 ± 0.5 m a.s.l. (Fig. 10e). We attribute to the 118 ka sea-level stillstand the deposition of coarse arenite with gravels of U2, which mantled the *C. caespitosa* bioherm and probably also partly reworked the U1. Finally, the sea level dropped at the end of MIS 5e (after 118 ka in our modelling). To this phase and the following periods, we attribute continental units U3 and U4, which indicate a coastline progressively retreating farther away (Fig. 10f). The absence of other marine units lying stratigraphically above U3 and U4 confirms the absence of any further sea highstands above present-day sea level during subsequent MIS 5 sub-stages in the study area, as already concluded in Isola et al. (2024). Nevertheless, in the Tyrrhenian coastal sector of the Basilicata and northern Calabria, ca. 30 km to the SE of our study area (between Maratea and Scalea), Cerrone et al. (2021b) reconstructed the elevations of MIS 5a and 5c sea level peaks, finding them to be higher than those reported in most sea-level curves worldwide and consistent with observations from the western Mediterranean. For instance, the reconstructed elevation of MIS 5a along the Tyrrhenian coast of northern Calabria-Basilicata is ca. 2 m a.s.l., and future

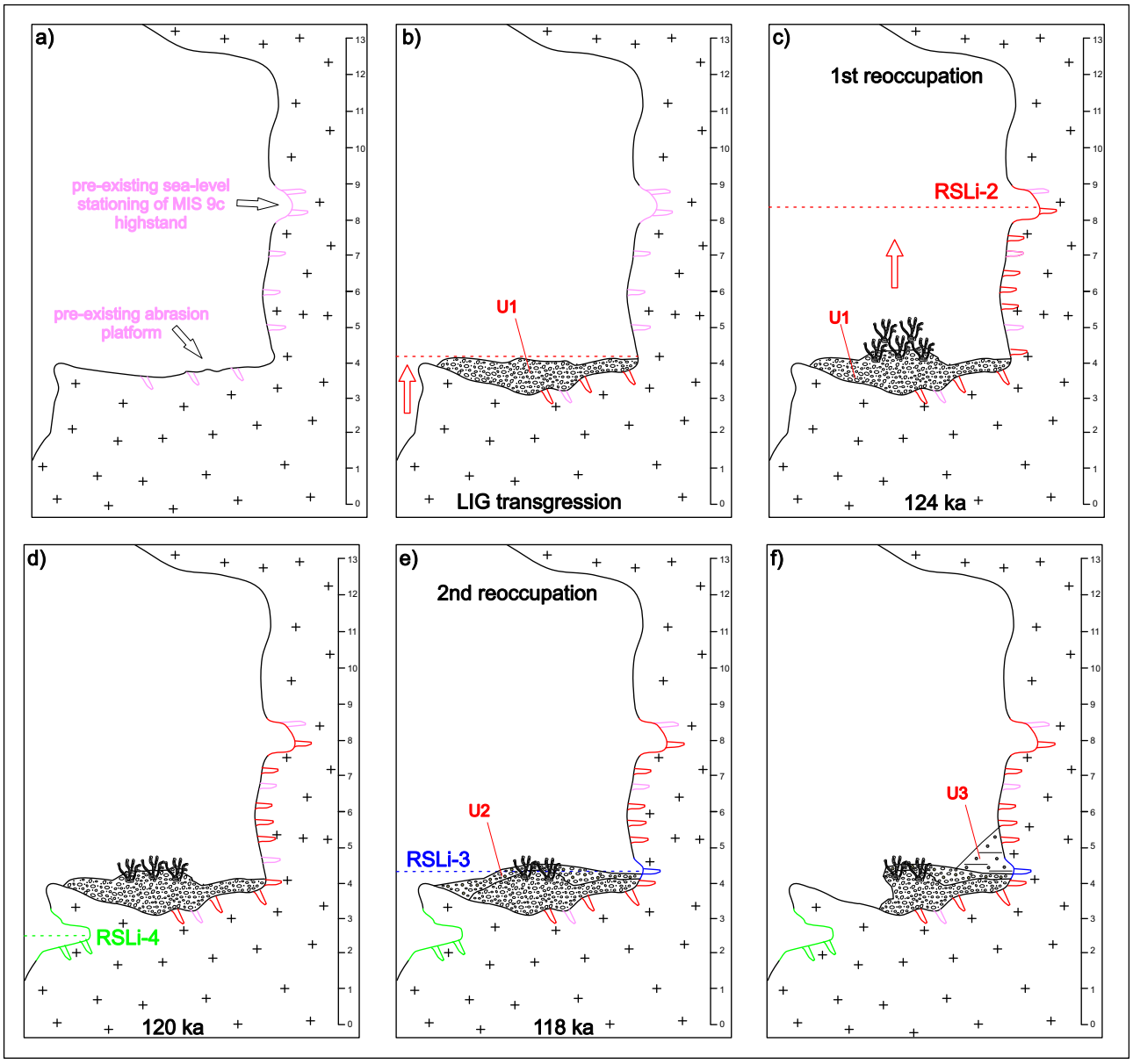

Fig. 10. Reconstruction of sea level oscillations in the Coral Cave site. (a) Pre-MIS 5e Transgression: At the Coral Cave site, before the MIS 5e transgression, the paleo sea-level peak of MIS 9c was already established (Isola et al., 2024). The platform at 4 ± 0.5 m a.s.l., dating back to an undefined stage, was also present. (b) MIS 5e Transgression: During the transgression of MIS 5e, the sea level reached the existing platform at 4 ± 0.5 m a.s.l., leading to the formation of U1. (c) First MIS 5e highstand: the first highstand of MIS 5e reoccupied the earlier MIS 9c RSLi. During this phase, the *C. caespitosa* bioherm formed above U1. (d) Second MIS 5e sea-level stillstand: the sea level dropped to form RSLi-4. During this phase, the *C. caespitosa* bioherm may have undergone early diagenesis and partial erosion in a subaerial environment. (e) The third and last sea-level stillstand of MIS 5e formed RSLi-3 with the reoccupation of the previously formed platform at 4 ± 0.5 m a.s.l. To this phase, we attribute the deposition of coarse arenite with gravels of U2, which mantled the *C. caespitosa* bioherm. (f) Deposition of aeolian sand above U1 and U2, and partial erosion of previously formed r deposits. This can be considered also the present-day situation. Along the wall of the cave, *Lithophaga* burrows were drawn with different colours in relation to the supposed phase of their formation.

investigations might reveal the occurrence of MIS 5a marine deposits also in our study area. It is also plausible that the lower sea level stillstand at 2.5 m a.s.l. (RSLi-4) could be correlated with MIS 5a.

5.3. Further local stratigraphic implications

Our results have significant local implications. At this scale, the concept of "reoccupation" of sea-level highstands is essential for investigating RSL indicators in regions with relatively low rates of crustal deformation. Our findings highlight that in such areas, older sea-level indicators may be reoccupied or overprinted by younger ones. This emphasizes the need for careful consideration of reoccupation processes to avoid erroneous interpretation of RSLi data. Accurate identification and dating of sea-level markers are essential for understanding past sea-level changes and their implications for coastal evolution in these regions.

Although our modelling provides a possible explanation and chronological attribution for the complex geomorphological features related to sea-level oscillations, some questions remain open and unsolved when we compare our model with existing field data.

Notably, none of the chronological data obtained so far in the study area directly refers to continental or marine units (Bini et al., 2020; Isola et al., 2024). On the contrary, the available ages refer to speleothem which have been used to indirectly constrain the marine and continental

units recognised. The only exception is the marine conglomerate (LU-3 in Bini et al., 2020 and Isola et al., 2024, corresponding to our U1), dated using marine fossil shells with scattered results between ~77 and ~ 145 ka (Bini et al., 2020).

Some unresolved issues arise from field data, and they need to be compared with (and possibly explained in the light of) our model.

Those issues are outlined below, along with potential explanations:

1) The reoccupation of RSLi-2 during the first MIS 5e highstand may have led to the drilling of speleothems by *Lithophaga*, Such speleothems are located at elevations lower than 8 m a.s.l and dated at MIS 6–8 interval in the Infreschi Cave and Infreschi Bay (Isola et al., 2024). However, it is important to note that *Lithophaga* is not required to drill surfaces in a spatially uniformly manner. Therefore, it is possible that, during the first MIS 5e highstand, the speleothems dated to MIS 6–8 intervals were not drilled by *Lithophaga*. Alternatively, these speleothems may have been initially covered by continental deposits that were later eroded.
2) The reoccupation of RSLi-3 during the last stillstand of MIS 5e (118 ka) may have caused the dismantling of the *C. caespitosa* bioherm, as this bioherm can be correlated with the first highstand of MIS 5e at RSLi-2 position (124 ka). However, this bioherm likely underwent a phase of emergence under subaerial conditions, followed by early diagenesis, between the stillstands forming RSLi-2 and RSLi-4 (Fig. 10d). This phase of early diagenesis may have played a crucial role in its preservation during the third and final sea-level stillstand at the RSLi-3 position. Alternatively, a decrease in hydrodynamic activity during this sea-level stillstand could have facilitated the preservation of the bioherm, as indicated by the finer sediments of U2 that now cover it.
3) When was the platform at Infreschi Cave, located at 4 ± 0.5 m a.s.l. and later reoccupied by the third sea-level peak of MIS 5e at RSLi-3 position, initially formed?

Regarding this question, we propose two hypotheses based on literature data about LIG and MIS 11: (i) an Early MIS 5e Sea-Level Stillstand and (ii) an Older Highstands (MIS 11):

(i) The platform may have initially formed during an early sea-level stillstand of the MIS 5e highstand. This potential stillstand might not be captured by the intra-LIG sea-level curve of Kopp et al. (2013), which was used in our model and aligns best with the field data. Some authors suggest the existence of a brief early sea-level stillstand before the higher peak of the LIG (Amorosi et al., 2014; Rohling et al., 2019);
(ii) Alternatively, the platform's initial formation could be associated with earlier highstands, such as those during MIS 11, which are not resolved in the sea-level curve of Waelbroeck et al. (2002), used in our model for all highstands except MIS 5e. For instance, some authors report the presence of substages MIS 11a and MIS 11c, (Shakun et al., 2015; Spratt and Lisiecki, 2016; Tzedakis et al., 2022).

4) In our reconstruction, we assume that the third and last sea-level stillstand of MIS 5e occurred at 118 ka. However, this assumption is somewhat at odds with the age of the speleothem sample POZZ22-1 reported by Isola et al. (2024) from Pozzallo, which was not investigated in the present study. This sample (a speleothem covering a marine deposit at ca. 1.5 m a.s.l.), yielded an age of 119.8 ± 0.8 ka, suggesting the sea level in the area had already definitively dropped by around 119 ka. On the other hand, the existence of a third sea-level stillstand of MIS 5e at 118 ka is partially supported by other chronological data from Bini et al. (2020) and Isola et al. (2024) (samples INF18/4, INF18/4A, INF18/4B, and INF20-5), which come from the only site in common with our study, namely Infreschi Bay. However, the difference between our modelled chronology and the field datum from speleothem sample POZZ22-1 (Isola et al., 2024) is small. Therefore, a possible reconciliation may be achieved considering the ranges of uncertainties in the chronology of intra-LIG sea-level stillstands by Kopp et al. (2013) and the uncertainty in the dating reported in Isola et al. (2024). On the other hand, the chronological data from Bini et al. (2020) and Isola et al. (2024) in partial agreement with our reconstruction, include:
   (i) three U/Th dates from calcite in *Lithophaga* holes reported by Bini et al. (2020) in the Infreschi Cave (samples INF18/4, INF18/4A, INF18/4B): these three dates range around ca. 120 ka and come from samples located around 3.7–3.8 m a.s.l. These three dates demonstrate that, at Infreschi Cave, the sea level, at 120 ka, was dropped below the present elevation of 3.7–3.8 m a.s.l. Our reconstruction, at the near site Coral Cave, of a third and last sea-level stillstand during MIS 5e, attained at 118 ka at a present mean elevation of 4 m a.s.l., could be reconciled with the chronological data by Bini et al. (2020) assuming that the deposition of calcite within the *Lithophaga* holes occurred during the subaerial exposure lasted from the late phase of regression after the first sea-level highstand of MIS 5e and the last sea-level stillstand of MIS 5e at 118 ka (Fig. 10d);
   (ii) Two U/Th dates from speleothems reported by Isola et al. (2024) in the Infreschi Bay, near Infreschi Cave (sample INF20-5): This sample, located at 3.5 m a.s.l., gave 2 dates: 108.2 ± 8.2 and 112.4 ± 6.0. These two dates demonstrate that the sea level dropped below the present elevation of 3.5 m a.s.l. at 112–108 ka at Infreschi Cave. This is in full agreement with our reconstruction.

5.4. Comparison with global data

On a global scale, our results can contribute to refining sea-level reconstructions and understanding regional variations in sea-level history. By demonstrating that reoccupation can occur, especially in tectonically stable areas, our study provides insights that can be applied to other regions with similar conditions. This has broader implications for interpreting past sea-level changes, calibrating sea-level curves, and understanding the interactions between sea level, tectonics, and climate across different geographic areas.

In particular, our case study suggests that more than one sea-level stillstand may have occurred during the LIG and that the best model to explain the observed RSLi implies three intra-LIG sea-level stillstands. These findings are important for studies that use indicators of MIS 5e, impacting research related to both tectonics and sea-level changes globally. In addition, our modelling points to a rapid drop in sea level after the first sea-level highstand, thus before 120 ka: we refer to the passage between RSLi-2 and the chronologically following RSLi-4 (Fig. 10). The same event, although with small chronological differences, has also been reported by other recent works in the Central Mediterranean realm (Bini et al., 2020; Isola et al., 2024; De Santis et al., 2024; Giaccio et al., 2024).

6. Conclusions

This work presents a model of RSL indicators, based on assumptions and morphostratigraphic evidence gathered in the field. It is the first attempt to assign ages to previously undated late Quaternary RSLi in a quasi-stable region such as the Mt. Bulgheria area (Ascione and Romano, 1999; Ferranti et al., 2006).

The modelling is based on the application of the synchronous method. For this method, highstands from sea-level curves have been introduced as inputs. The second input is an uplift rate of the study area. The uplift rate was derived from the assumption that RSLi-2 is correlated with MIS 9c, according to the conclusions of Isola et al. (2024). So, we tested different sea-level curves to achieve the best match between

observed and predicted sea-level highstands. The final best-fitting scenario was obtained using a composite sea-level curve, combining Waelbroeck et al. (2002) and Kopp et al. (2013), the latter limited to the last interglacial period. Among the global sea-level curves focused on LIG currently available, the one by Kopp et al. (2013) is best suited to explain the sea-level indicators observed in the study area, while also incorporating the most recent chronological constraints from Bini et al. (2020) and Isola et al. (2024).

Our model involved a constant uplift rate of 0.009 mm/yr from MIS 11. However, although the marine terrace at 150 m a.s.l. has been broadly attributed to the Middle Pleistocene, this attribution has never been supported by any direct chronological data. Hence, we cannot exclude the possibility that the Bulgheria Mountain area experienced a gradual reduction in the uplift rate during the Middle Pleistocene.

Our approach reveals a double case of reoccupation of previous sea-level stillstands by subsequent ones. In particular, we provide field evidence of the reoccupation of (i) the first MIS 5e highstand (124 ka) on MIS 9c at c. 8 m a.s.l., and (ii) of the last MIS 5e stillstand (118 ka) on an undefined older highstand at c. 4 m a.s.l.

Our reconstruction supports the hypothesis that both MIS 9 and MIS 11 had sea levels higher than the present. This aligns with sea-level curves by Waelbroeck et al. (2002), Siddall et al. (2003, for MIS 9), Spratt and Lisiecki (2016, for MIS 11) and specific studies on these MISs (Roberts et al., 2012; Reyes et al., 2014; Dutton et al., 2015; Robinson et al., 2017; Tzedakis et al., 2022).

In contrast, this work does not support reconstructions of MIS 9 and 11 sea levels being similar to or lower than present. This contrasts with other sea-level curves (Siddall et al., 2003, for MIS 11; Rohling et al., 2009; Grant et al., 2014; Spratt and Lisiecki, 2016, for MIS 9) and specific studies on these isotopic stages (e.g., Bowen, 2010).

On the regional scale, our work is in agreement with findings of stromatolitic deposits in Apulia (southern Italy) dating to MIS 9 and MIS 11, which allowed reconstructing paleotemperatures higher than the present for these two isotopic stages (De Santis et al., 2014), which in turn would imply sea levels higher than the present.

Finally, this work emphasizes the importance of not assuming, where age constraints are lacking, that RSL indicators at an elevation up to ca. 8 m a.s.l., in tectonically stable areas, were exclusively formed during MIS 5e, especially.

CRediT authorship contribution statement

Vincenzo De Santis: Writing – review & editing, Writing – original draft, Visualization, Validation, Software, Resources, Methodology, Investigation, Funding acquisition, Formal analysis, Data curation, Conceptualization. **Ciro Cerrone:** Writing – review & editing, Writing – original draft, Visualization, Validation, Resources, Methodology, Investigation, Formal analysis, Data curation, Conceptualization. **Marco Meschis:** Writing – review & editing, Software, Formal analysis. **Giovanni Scicchitano:** Writing – review & editing, Supervision. **Alessandra Ascione:** Writing – review & editing, Visualization, Supervision. **Massimo Caldara:** Writing – review & editing, Visualization, Supervision, Resources, Formal analysis, Investigation, Funding acquisition.

Financial support

This work was supported by the Italian Association for the Study of Quaternary (AIQUA) and Italian Alpine Club (CAI), who awarded a Grant Ciro Cerrone for the Quaternary studies on the central-southern Apennines. This paper is a result of the WARMCOAST proeject, funded by the European Research Council (ERC) under the European Union's Horizon 2020 research and innovation programme (Grant agreement No. 802414). This paper reflects only the author's view and that the EU is not responsible for any use that may be made of the information it contains.

Open access publishing was facilitated by the University of Venice Ca' Foscari as part of the Elsevier - CRUI-CARE agreement.

Declaration of competing interest

The authors declare that they have no known competing financial interests or personal relationships that could have appeared to influence the work reported in this paper.

Acknowledgements

The authors acknowledge PALSEA, a working group of the International Union for Quaternary Sciences (INQUA) and Past Global Changes (PAGES), which in turn received support from the Swiss Academy of Sciences and the Chinese Academy of Sciences.

The authors acknowledge also Prof. Giuseppina Balassone (Department of Earth, Environmental and Resources Science, University of Naples Federico II) for XRD analyses on Cladocora caespitosa samples and Prof. Vitantonio Crismale and Sefano Rossi (Department of Mathematics, University of Bari Aldo Moro) for the fruitful discussions regarding linear regression and R^2.

We are very grateful to Raffaele Ruocco, Mario D'Angelo and Coop. Cilento Mare for their logistical support during the field survey.

Appendix A. Supplementary data

Supplementary data to this article can be found online at https://doi.org/10.1016/j.geomorph.2025.109692.

Data availability

Data will be made available on request.

References

Amorosi, A., Antonioli, F., Bertini, A., Marabini, S., Mastronuzzi, G., Montagna, P., Negri, A., Rossi, V., Scarponi, D., Taviani, M., Angeletti, L., Piva, A., Vai, G.B., 2014. The Middle-Upper Pleistocene Fronte Section (Taranto, Italy): an exceptionally preserved marine record of the last interglacial. Global Planet. Change 119, 23–38.

Antonioli, F., Ferranti, L., Lambeck, K., Kershaw, S., Verrubbi, V., Dai Pra, G., 2006. Late Pleistocene to Holocene record of changing uplift rates in southern Calabria and northeastern Sicily (southern Italy, Central Mediterranean Sea). Tectonophysics 422, 23–40. https://doi.org/10.1016/j.tecto.2006.05.003.

Armijo, R., Meyer, B., King, G.C.P., Rigo, A., Papanastassiou, D., 1996. Quaternary evolution of the Corinth Rift and its implications for the Late Cenzoic evolution of the Aegean. Geophys. J. Int. 126 (1), 11–53. https://doi.org/10.1111/j.1365-246X.1996.tb05264.x.

Ascione, A., Romano, P., 1999. Vertical movements on the eastern margin of the Tyrrhenian extensional basin. New data from Mt. Bulgheria (Southern Apennines, Italy). Tectonophysics 315, 337–356. https://doi.org/10.1016/S0040-1951(99)00279-6.

Bardají, T., Goy, J.L., Zazo, C., Hillaire-Marcel, C., Dabrio, C.J., Cabero, A., Ghaleb, B., Silva, P.G., Lario, J., 2009. Sea level and climate changes during OIS 5e in the Western Mediterranean. Geomorphology 104, 22–37. https://doi.org/10.1016/j.geomorph.2008.05.027.

Benjamin, J., Rovere, A., Fontana, A., Furlani, S., Vacchi, M., Inglis, R.H., Galili, E., Antonioli, F., Sivan, D., Miko, S., Mourtzas, N., Felja, I., Meredith-Williams, M., Goodman-Tchernov, B., Kolaiti, E., Anzidei, M., Gehrels, R., 2017. Late Quaternary sea-level changes and early human societies in the central and eastern Mediterranean Basin: an interdisciplinary review. Quat. Int. 449, 29–57. https://doi.org/10.1016/j.quaint.2017.06.025.

Bini, M., Zanchetta, G., Drysdale, R.N., Giaccio, B., Stocchi, P., Vacchi, M., Hellstrom, J. C., Couchoud, I., Monaco, L., Ratti, A., Martini, F., Sarti, L., 2020. An end to the last interglacial highstand before 120 ka: relative sea-level evidence from Infreschi Cave (southern Italy). Quat. Sci. Rev. 250, 106658. https://doi.org/10.1016/j.quascirev.2020.106658.

Bowen, D.Q., 2010. Sea level ~400 000 years ago (MIS 11): analogue for present and future sea-level? Clim. Past 6, 19–29.

Caiazzo, C., Ascione, A., Cinque, A., 2006. Late Tertiary-Quaternary tectonics of the Southern Apennines (Italy): new evidences from the Tyrrhenian slope. Tectonophysics 421, 23–51. https://doi.org/10.1016/j.tecto.2006.04.011.

Cerrone, C., Vacchi, M., Fontana, A., Rovere, A., 2021a. Last Interglacial sea-level proxies in the western Mediterranean. Earth Syst Sci Data 13, 4485–4527. https://doi.org/10.5194/essd-13-4485-2021.

Cerrone, C., Ascione, A., Robustelli, G., Tuccimei, P., Soligo, M., Balassone, G., Mormone, A., 2021b. Late Quaternary uplift and sea level fluctuations along the

Tyrrhenian margin of Basilicata - northern Calabria (southern Italy): new constraints from raised paleoshorelines. Geomorphology 395, 107978.
Cerrone, C., Meschis, M., Ascione, A., Soligo, M., Tuccimei, P., Robertson, J., Roberts, G. P., 2025. Tectonic implications of raised Quaternary relative sea-level indicators along the NE border of the Campania Plain (Southern Italy). Earth Surf. Process. Landforms. 50 (1), e6066. https://doi.org/10.1002/esp.6066.
Chauveau, D., Authemayou, C., Pedoja, K., Molliex, S., Husson, L., Scholz, D., Godard, V., Pastier, A.-M., de Gelder, G., Cahyarini, S.Y., Elliot, M., Weber, M., Benedetti, L., Jaud, M., Boissier, A., Agusta, V.C., Aribowo, S., Budd, A.F., Natawidjaja, D.H., 2021. On the generation and degradation of emerged coral reef terrace sequences: first cosmogenic 36Cl analysis at Cape Laundi, Sumba Island (Indonesia). Quaternary Science Reviews 269, 107144. https://doi.org/10.1016/j.quascirev.2021.107144.
Chauveau, D., Georgiou, N., Cerrone, C., Dean, S., Rovere, A., 2024. Sea-level oscillations within the last interglacial: insights from coral reef stratigraphic forward modelling. Quat. Sci. Rev. 336, 108759. https://doi.org/10.1016/j.quascirev.2024.108759.
Cinque, A., Romano, P., 1990. Segnalazione di nuove evidenze di antiche linee di riva in Penisola Sorrentina (Campania). Geogr. Fis. Din. Quat. 13, 23–36.
Cita, Maria Bianca, Capraro, Luca, Ciaranfi, Neri, Di Stefano, Enrico, Marino, Maria, Rio, Domenico, Sprovieri, Rodolfo, Vai, Gian Battista, 2006. Calabrian and Ionian: a proposal for the definition of Mediterranean stages for the Lower and Middle Pleistocene. Episodes 29 (2), 107–114. https://doi.org/10.18814/epiiugs/2006/v29i2/004.
Cohen, K.M., Gibbard, P.L., 2019. Global chronostratigraphical correlation table for the last 2.7 million years, version 2019 QI-500. Quat. Int. 500, 20–31. https://doi.org/10.1016/j.quaint.2019.03.009.
Crosetto, S., de Montserrat, A., Oncken, O., 2024. Uplifted Pleistocene marine terraces at active margins: modeling reveals the effects of sea reoccupation and coseismic uplift on uplift rate calculation. Geochem. Geophys. Geosyst. 25. https://doi.org/10.1029/2023GC011036.
De Santis, V., Caldara, M., Torres, T., Ortiz, E., 2014. Two middle Pleistocene warm stages in the Terraced Deposits of the Apulia Region (southern Italy). Quat. Int. 332, 2–18.
De Santis, V., Scardino, G., Meschis, M., Ortiz, J.E., Sánchez-Palencia, Y., Caldara, M., 2021. Refining the middle-late Pleistocene chronology of marine terraces and uplift history in a sector of the Apulian foreland (southern Italy) by applying a synchronous correlation technique and amino acid racemization to Patella spp. and Thetystrombus latus. Ital. J. Geosci. 140, 438–463. https://doi.org/10.3301/IJG.2021.05.
De Santis, V., Scardino, G., Scicchitano, G., Meschis, M., Montagna, P., Pons-Branchu, E., Ortiz, J.E., Sánchez-Palencia, Y., Caldara, M., 2023. Middle-late Pleistocene chronology of palaeoshorelines and uplift history in the low-rising to stable Apulian foreland: overprinting and reoccupation. Geomorphology 421, 108530. https://doi.org/10.1016/j.geomorph.2022.108530.
De Santis, V., Montagna, P., Scicchitano, G., Mastronuzzi, G., Pons-Brancu, E., Scardino, G., Ortiz, J.E., Sanchez-Palencia, Y., Torres, T., Caldara, M., 2024. Two main highstands during the Last Interglacial: insights from palaeoshorelines and marine terraced deposits along the Ionian coast of the Apulia region, Southern Italy. Earth Surf. Process. Landf. https://doi.org/10.1002/esp.5912.
Dumitru, O.A., Polyak, V.J., Asmerom, Y., Onac, B.P., 2021. Last interglacial sea-level history from speleothems: a global standardized database. Earth Syst. Sci. Data 13, 2077–2094. https://doi.org/10.5194/essd-13-2077-2021.
Dutton, A., Lambeck, K., 2012. Ice volume and sea level during the last interglacial. Science 337, 216–219. https://doi.org/10.1126/science.1205749.
Dutton, A., C., A.E., Long, A.J., Milne, G.A., Clark, P.U., DeConto, R., Horton, B.P., Rahmstorf, S., Raymo, M.E., 2015. Sea-level rise due to polar ice-sheet mass loss during past warm periods. Science 349, aaa4019.
Dyer, B., Austermann, J., D'Andrea, W.J., Creel, R.C., Sandstrom, M.R., Cashman, M., Rovere, A., Raymo, M.E., 2021. Sea-level trends across the Bahamas constrain peak last interglacial ice melt. Proc. Natl. Acad. Sci. U. S. A. 17 (33), 118. https://doi.org/10.1073/pnas.2026839118.
Esposito, C., Filocamo, F., Marciano, R., Romano, P., Santangelo, N., Scarciglia, P., Tuccimei, P., 2003. Late Quaternary shorelines in southern Cilento (Mt. Bulgheria): morphostratigraphy and chronology. Alpine and Mediterranean Quaternary 16 (1), 3–14. https://amq.aiqua.it/index.php/amq/article/view/587.
Faccenna, C., Becker, T.W., Lucente, F.P., Jolivet, L., Rossetti, F., 2001a. History of subduction and back-arc extension in the Central Mediterranean. Geophys. J. Int. 145, 809–820.
Faccenna, C., Funiciello, F., Giardini, D., Lucente, P., 2001b. Episodic back-arc extension during restricted mantle convection in the Central Mediterranean. Earth Planet Science Letters 187, 105–116.
Ferranti, L., Antonioli, F., 2007. Misure del solco Tirreniano (MIS 5.5) nell'isola di Capri: valutazione di attività tettonica durante il Pleistocene superiore. Il Quaternario 20 (2), 125–136.
Ferranti, L., Antonioli, F., Mauz, B., Amorosi, A., Dai Pra, G., Mastronuzzi, G., Monaco, C., Orru, P., Pappalardo, M., Radtke, U., Renda, P., Romano, P., Sansò, P., Verrubbi, V., 2006. Markers of the last interglacial sea-level high stand along the coast of Italy: tectonic implications. Quat. Int. 145-146, 30–54.
Filocamo, F., 2000. Geomorfologia e stratigrafia del tardo Quaternario al Monte Bulgheria (Cilento Meridionale) (Master's Thesis).
Giaccio, B., Bini, M., Isola, I., Hu, H., Rolfo, M.F., Shen, C., Ferracci, A., Monaco, L., Pasquetti, F., Zanchetta, G., 2024. Constraining the end of the Last Interglacial (MIS 5e) relative sea level highstand in central Mediterranean: New data from Grotta delle Capre, central Italy. Global Planet. Change 232, 104321. https://doi.org/10.1016/j.gloplacha.2023.104321.
Gibbard, Philip L., Head, Martin J., 2009. The definition of the quaternary system/era and the Pleistocene series/epoch. Quaternaire no. vol. 20/2 (June), 125–133. https://doi.org/10.4000/quaternaire.5086.
Grant, K.M., Rohling, E.J., Rohling, E.J., Ramsey, C.B., Cheng, H., Cheng, H., Edwards, R. L., Florindo, F., Heslop, D., Marra, F., Roberts, A.P., Tamisiea, M.E., Williams, F.H., 2014. Sea-level variability over five glacial cycles. Nat. Commun. 5.
Houghton, S.L., Roberts, G.P., Papanikolaou, I.D., McArthur, J.M., 2003. New 234 U- 230 Th coral dates from the western Gulf of Corinth: implications for extensional tectonics. Geophys. Res. Lett. 30, 2013. https://doi.org/10.1029/2003GL018112.
Iannace, A., Romano, P., Santangelo, N., Santo, A., Tuccimei, P., 2001. The OIS 5c along Licosa cape promontory (Campania region, southern Italy): morphostratigraphy and U/Th dating. Zeitschrift für Geomorphologie N.F. 45 (3), 307–319.
Iannace, A., Romano, P., Tuccimei, P., 2003. U/Th dating and geochemistry of carbonate concretions associated with upper Pleistocene fossil shorelines of the Sorrento Peninsula (Conca dei Marini, southern Italy). Il Quaternario - Italian Journal of Quaternary Sciences 6 (1Bis), 49–54.
IPCC, 2023. Climate change 2023: synthesis report. In: Core Writing Team, Lee, H., Romero, J. (Eds.), Contribution of Working Groups I, II and III to the Sixth Assessment Report of the Intergovernmental Panel on Climate Change. IPCC, Geneva, Switzerland, pp. 35–115. https://doi.org/10.59327/IPCC/AR6-9789291691647.
Isola, I., Bini, M., Columbu, A., Di Vito, M.A., Giaccio, B., Hu, H., Martini, F., Pasquetti, F., Sarti, L., Mule, F., Mazzoleni, A., Shen, C., Zanchetta, G., 2024. Last Interglacial and MIS 9e relative sea-level highstands in the Central Mediterranean: a reappraisal from coastal cave deposits in the Cilento area, Southern Italy. Quaternary Science Advances 15, 100212.
ISPRA, 2016. Foglio 520 Sapri della Carta Geologica d'Italia alla scala 1:50.000. ISPRA, Roma. https://www.isprambiente.gov.it/Media/carg/520_SAPRI/Foglio.html.
Kopp, R.E., Simons, F.J., Mitrovica, J.X., Maloof, A.C., Oppenheimer, M., 2009. Probabilistic assessment of sea level during the last interglacial stage. Nature 462, 863–867. https://doi.org/10.1038/nature08686.
Kopp, R.E., Simons, F.J., Mitrovica, J.X., Maloof, A.C., Oppenheimer, M., 2013. A probabilistic assessment of sea level variations within the last interglacial stage. Geophys. J. Int. 193, 711–716.
Kružić, P., Požar-Domac, A., 2003. Banks of the coral Cladocora caespitosa (Anthozoa, Scleractinia) in the Adriatic Sea. Coral Reefs 22, 536.
Lambeck, K., Woodroffe, C.D., Antonioli, F., Anzidei, M., Gehrels, W.R., Laborel, J., Wright, A.J., 2010. Paleoenvironmental records, geophysical modeling, and reconstruction of sea-level trends and variability on centennial and longer timescales. In: Understanding Sea-Level Rise and Variability. Wiley, pp. 61–121. https://doi.org/10.1002/9781444323276.ch4.
Lorscheid, T., Stocchi, P., Casella, E., Gómez-Pujol, L., Vacchi, M., Mann, T., Rovere, A., 2017. Paleo sea-level changes and relative sea-level indicators: precise measurements, indicative meaning and glacial isostatic adjustment perspectives from mallorca (western mediterranean). Palaeogeogr. Palaeoclimatol. Palaeoecol. 473, 94107. https://doi.org/10.1016/j.palaeo.2017.02.028.
Malinverno, A., Ryan, W.B.F., 1986. Extension in the Tyrrhenian Sea and shortening in the Apennines as result of arc migration driven by sinking of the lithosphere. Tectonics 5, 227–245. https://doi.org/10.1029/TC005i002p00227.
Meschis, M., Roberts, G.P., Robertson, J., Briant, R.M., 2018. The relationships between regional quaternary uplift, deformation across active normal faults, and historical seismicity in the upper plate of subduction zones: the Capo D'Orlando Fault, NE Sicily. Tectonics 37, 1231–1255. https://doi.org/10.1029/2017TC004705.
Meschis, M., Romano, D., Palano, M., Scicchitano, G., De Santis, V., Scardino, G., Gattuso, A., Caruso, C.G., Sposito, F., Lazzaro, G., Scappuzzo, S.S.S., Semprebello, A., Morici, S., Longo, M., 2024. Crustal uplift rates implied by synchronously investigating Late Quaternary marine terraces in the Milazzo Peninsula, Northeast Sicily, Italy. Earth Surf. Process. Landf. 49, 3555–3574. https://doi.org/10.1002/esp.5922.
Meschis, M., Scicchitano, G., Roberts, G.P., Robertson, J., Barreca, G., Monaco, C., Spampinato, C., Sahy, D., Antonioli, F., Mildon, Z.K., Scardino, G., 2020. Regional deformation and offshore crustal local faulting as combined processes to explain uplift through time constrained by investigating differentially-uplifted Late Quaternary palaeoshorelines: the foreland Hyblean Plateau, SE Sicily. Tectonics. https://doi.org/10.1029/2020TC006187.
Meschis, M., Roberts, G.P., Robertson, J., Mildon, Z.K., Sahy, D., Goswami, R., Sgambato, C., Walker, J.F., Michetti, A.M., Iezzi, F., 2022a. Out of phase Quaternary uplift-rate changes reveal normal fault interaction, implied by deformed marine palaeoshorelines. Geomorphology 416, 108432. https://doi.org/10.1016/j.geomorph.2022.108432.
Meschis, M., Teza, G., Serpelloni, E., Elia, L., Lattanzi, G., Di Donato, M., Castellaro, S., 2022b. Refining rates of active crustal deformation in the upper plate of subduction zones, implied by geological and geodetic data: the E-Dipping West Crati Fault, Southern Italy. Remote Sensing 14, 5303. https://doi.org/10.3390/rs14215303.
Montagna, P., Silenzi, S., Devoti, S., Mazzoli, C., McCulloch, M., Scicchitano, G., Taviani, M., 2008. Climate reconstructions and monitoring in the Mediterranean Sea: a review on some recently discovered high-resolution marine archives. Rendiconti Lincei. https://doi.org/10.1007/s12210-008-0007-7.
Moussat, E., Rehault, J.P., Fabbri, A., 1986. Rifting et évolution tectono-sèdimentaire du Bassin Tyrrhènien au cours du Neogene et du Quaternaire. Giorn. di Geol. Serie 3 (48), 41–62, 1/2.
Murray-Wallace, C.V., Woodroffe, C.D., 2014. Quaternary Sea-Level Changes: A Global Perspective. Cambridge University Press, Cambridge, United Kingdom.
Patacca, E., Scandone, P., 2001. Late thrust propagation and sedimentary response in the thrust-belt—foredeep system of the Southern Apennines (Pliocene-Pleistocene). In:

Anatomy of an Orogen: the Apennines and Adjacent Mediterranean Basins, pp. 401–440. https://doi.org/10.1007/978-94-015-9829-3_23.
Patacca, E., Sartori, R., Scandone, P., 1990. Tyrrhenian basin and Apenninic Arcs: kinematic relations since Late Tortonian times. Mem. Soc. Geol. It 45, 425–451. https://doi.org/10.1007/978-94-011-2016-6_7.
Pedoja, K., Jara-Muñoz, J., De Gelder, G., Robertson, J., Meschis, M., Fernandez-Blanco, D., Nexer, M., Poprawski, Y., Dugué, O., Delcaillau, B., Bessin, P., Benabdelouahed, M., Authemayou, C., Husson, L., Regard, V., Menier, D., Pinel, B., 2018. Neogene-Quaternary slow coastal uplift of Western Europe through the perspective of sequences of strandlines from the Cotentin Peninsula (Normandy, France). Geomorphology 303, 338–356. https://doi.org/10.1016/j.geomorph.2017.11.021.
Peirano, A., Morri, C., Bianchi, C.N., Aguirre, J., Antonioli, F., Calzetta, G., Carobene, L., Mastronuzzi, G., Orrù, P., 2003. The Mediterranean coral Cladocora caespitosa: a proxy for past climate fluctuations? Global Planet. Change 40, 195–200.
Perazzotti, F., Del Valle, L., Fornós, J.J., 2024. An overview of Upper Pleistocene coastal deposits on Mallorca island. Quat. Int. 707, 60–71. https://doi.org/10.1016/j.quaint.2024.07.013.
Rehault, J.P., Moussat, E., Fabbri, A., 1987. Structural evolution of the Tyrrhenian back-arc basin. Mar. Geol. 74, 123–150.
Reyes, A.V., Carlson, A.E., Beard, B.L., Hatfield, R.G., Stoner, J.S., Winsor, K., Welke, B., Ullman, D.J., 2014. South Greenland ice-sheet collapse during Marine Isotope Stage 11. Nature 510, 525–528.
Riccio, A., Riggio, F., Romano, P., 2001. Sea level fluctuation during Oxygen Isotope Stage 5: new data from fossil shorelines in the Sorrento Peninsula (Southern Italy). Z. Geomorph. N.F. 45 (1), 121–137.
Roberts, G.P., Houghton, S.L., Underwood, C., Papanikolaou, I., Cowie, P.A., van Calsteren, P., Wigley, T., Cooper, F.J., McArthur, J.M., 2009. Localization of Quaternary slip rates in an active rift in 10 5 years: an example from Central Greece constrained by 234 U- 230 Th coral dates from uplifted paleoshorelines. J. Geophys. Res. 114 (B10), B10406. https://doi.org/10.1029/2008JB005818.
Roberts, D.L., Karkanas, P., Jacobs, Z., Marean, C.W., Roberts, R.G., 2012. Melting ice sheets 400,000 yr ago raised sea level by 13m: past analogue for future trends. Earth Planetary Science Letters 357-358, 226–237.
Roberts, G.P., Meschis, M., Houghton, S., Underwood, C., Briant, R.M., 2013. The implications of revised Quaternary palaeoshoreline chronologies for the rates of active extension and uplift in the upper plate of subduction zones. Quaternary Science Reviews 78, 169–187. https://doi.org/10.1016/j.quascirev.2013.08.006.
Robertson, J., Meschis, M., Roberts, G.P., Ganas, A., Gheorghiu, D.M., 2019. Temporally constant quaternary uplift rates and their relationship with extensional upper-plate faults in South Crete (Greece), constrained with 36Cl cosmogenic exposure dating. Tectonics 38. https://doi.org/10.1029/2018TC005410.
Robertson, J., Roberts, G.P., Iezzi, F., Meschis, M., Gheorghiu, D.M., Sahy, D., Bristow, C., Sgambato, C., 2020. Distributed normal faulting in the tip zone of the South Alkyonides Fault System, Gulf of Corinth, constrained using 36Cl exposure dating of late-Quaternary wave-cut platforms. J. Struct. Geol. 136, 104063. https://doi.org/10.1016/j.jsg.2020.104063.
Robertson, J., Roberts, G.P., Ganas, A., Meschis, M., Gheorghiu, D.M., Shanks, R.P., 2023. Quaternary uplift of palaeoshorelines in southwestern Crete: the combined effect of extensional and compressional faulting. Quaternary Science Reviews 316, 108240. https://doi.org/10.1016/j.quascirev.2023.108240.
Robinson, A., Alvarez-Solas, J., Calov, R., Ganopolski, A., Montoya, M., 2017. MIS-11 duration key to disappearance of the Greenland ice sheet. Nat. Commun. 8, 16008.
Rohling, E.J., Grant, K.M., Bolshaw, M., Roberts, A.P., Siddall, M.E., Hemleben, C., Kučera, M., 2009. Antarctic temperature and global sea level closely coupled over the past five glacial cycles. Nat. Geosci. 2, 500–504.
Rohling, E.J., Hibbert, F.D., Grant, K.M., Galaasen, E.V., Irvali, N., Kleiven, H.F., Marino, G., Ninnemann, U., Roberts, A.P., Rosenthal, Y., 2019. Asynchronous Antarctic and Greenland ice-volume contributions to the last interglacial sealevel highstand. Nat. Commun. 10, 5040.
Rovere, A., Antonioli, F., Bianchi, C.N., 2015. Chapter 18. Fixed biological indicators. In: Shennan, A., Horton, B.P. (Eds.), Handbook of Sea-Level Research. Wiley & Sons Ltd, pp. 268–280.
Rovere, A., Raymo, M.E., Vacchi, M., Lorscheid, T., Stocchi, P., Gomez-Pujol, L., Harris, D.L., Casella, E., O'Leary, M.J., Hearty, P.J., 2016. The analysis of Last Interglacial (MIS 5e) relative sea-level indicators: reconstructing sea-level in a warmer world. Earth Sci. Rev. 159, 404–427. https://doi.org/10.1016/j.earscirev.2016.06.006.
Royden, L.H., 1993. The tectonic expression slab pull at continental convergent boundaries. Tectonics 12, 303–325.
Royden, L., Patacca, E., Scandone, P., 1987. Segmentation and configuration of subducted lithosphere in Italy: an important control on thrust-belt and foredeep-basin evolution. Geology 15, 714–718.
Ruggieri, G., Selli, R., 1949. Il Pliocene ed il Postpliocene dell'Emilia. Giorn. Geol. (2) 20, 1–14.
Shakun, J.D., Lea, D.W., Lisiecki, L.E., Raymo, M.E., 2015. An 800-kyr record of global surface ocean d18O and implications for ice volume-temperature coupling. Earth Planetary Science Letters 426, 58–68.
Siddall, M.E., Rohling, E.J., Almogi-Labin, A., Hemleben, C., Meischner, D., Schmelzer, I., Smeed, D.A., 2003. Sea-level fluctuations during the last glacial cycle. Nature 423, 853–858.
Sivan, D., Sisma-Ventura, G., Greenbaum, N., Bialik, O.M., Williams, F.H., Tamisiea, M. E., Rohling, E.J., Frumkin, A., Avnaim-Katav, S., Shtienberg, G., Stein, M., 2016. Eastern Mediterranean sea levels through the last interglacial from a coastal-marine sequence in northern Israel. Quat. Sci. Rev. 145, 204–225. https://doi.org/10.1016/j.quascirev.2016.06.001.
Spratt, R.M., Lisiecki, L.E., 2016. A Late Pleistocene Sea level stack. Climate of the Past 12, 1079–1092.
Tzedakis, P.C., Hodell, D.A., Nehrbass-Ahles, C., Mitsui, T., Wolff, E.W., 2022. Marine Isotope Stage 11c: an unusual interglacial. Quaternary Science Reviews 284, 107493.
Vacchi, M., Ermolli, E.R., Morhange, C., Ruello, M.R., Di Donato, V., Di Vito, M.A., Boetto, G., 2020. Millennial variability of rates of sea-level rise in the ancient harbour of Naples (Italy, western Mediterranean Sea). Quat. Res. 93, 284–298.
Varzi, A.G., Meschis, M., Fallati, L., Scicchitano, G., De Santis, V., Scardino, G., Basso, D., Bracchi, V.A., Savini, A., 2024. New chronology for submerged relict paleoshorelines and associated rates of crustal vertical movements offshore the Marzamemi village, Sicily (Southern Italy). Mar. Geol. 474, 107326. https://doi.org/10.1016/j.margeo.2024.107326.
Vesica, P.L., Tuccimei, P., Turi, B., Fornós, J.J., Ginés, A., Ginés, J., 2000. Late Pleistocene Paleoclimates and sea-level change in the Mediterranean as inferred from stable isotope and U-series studies of overgrowths on speleothems, Mallorca, Spain. Quat. Sci. Rev. 19, 865–879. https://doi.org/10.1016/S0277-3791(99)00026-8.
Vitale, S., Ciarcia, S., 2018. Tectono-stratigraphic setting of the Campania region (southern Italy). J. Maps 14, 9–21. https://doi.org/10.1080/17445647.2018.1424655.
Waelbroeck, C., Labeyrie, L., Michel, E., Duplessy, J.C., McManus, J.F., Lambeck, K., Balbon, E., Labracherie, M., 2002. Sea-level and deep water temperature changes derived from benthic foraminifera isotopic records. Quaternary Science Reviews 21, 295–305. https://doi.org/10.1016/S0277-3791(01)00101-9.